Title:

Crossing thermal limits: functional collapse of the surfgrass *Phyllospadix scouleri* under extreme marine heatwaves

Running title:

Extreme marine heatwaves exceed seagrass thermal limits

Authors:

Manuel Vivanco-Bercovich[1*], Paula Bonet-Meliá[1], Nadine Schubert[2], Lázaro Marín-Guirao[3], Raquel Muñiz-Salazar[1,4], Alejandro Cabello-Pasini[1], Alejandra Ferreira-Arrieta[1], Jessica Anayansi Garcia-Pantoja[1], José Manuel Guzmán-Calderón[1], Gabriele Procaccini[5,6], Guillermo Samperio-Ramos[7], Jose M. Sandoval-Gil*[1,8]

Affiliations:

[1] Universidad Autónoma de Baja California (UABC), Instituto de Investigaciones Oceanológicas (IIO), Marine Botany Research Group, Ensenada, Baja California, México

[2] Centre of Marine Sciences (CCMAR/CIMAR LA), Campus de Gambelas, Universidade do Algarve, 8005-139 Faro, Portugal.

[3] Instituto Español de Oceanografía (IEO), Centro Oceanográfico de Murcia, Seagrass Ecology Group, C/Varadero s/n, 30740 San Pedro del Pinatar, Murcia, Spain.

[4] Universidad Autónoma de Baja California (UABC), Escuela de Ciencias de la Salud, Ensenada, Baja California, México

[5] Stazione Zoologica Anton Dohrn, Department of Integrative Marine Ecology, Villa Comunale, Naples, Italy.

[6] National Biodiversity Future Center, Palermo, Italy.

[7] Universidad Autónoma de Baja California (UABC), Instituto de Investigaciones Oceanológicas (IIO), Nutrient Cycling in Marine Ecosystems (CiNEMa) Research Group, Ensenada, Baja California, México.

[8] Laboratorio Nacional de Biología del Cambio Climático, SECIHTI, Ciudad de México, México.

***Corresponding authors:**

Jose Miguel Sandoval Gil - Universidad Autónoma de Baja California (UABC), Instituto de Investigaciones Oceanológicas, Carretera Ensenada-Tijuana No. 3917, Fraccionamiento Playitas. ZIP: 22860, Ensenada, Baja California, México | Tel: +52 1 646 138 9598 | jose.miguel.sandoval.gil@uabc.edu.mx | Orchid ID: 0000-0001-8973-0306

Manuel Vivanco Bercovich - Universidad Autónoma de Baja California (UABC), Instituto de Investigaciones Oceanológicas, Carretera Ensenada-Tijuana No. 3917, Fraccionamiento Playitas. ZIP: 22860, Ensenada, Baja California, México | Tel: +52 1 646 138 9598 | manuel.bercovich@uabc.edu.mx | Orchid ID: 0000-0003-1837-3465

Author email adresses:

Manuel Vivanco-Bercovich — manuel.bercovich@uabc.edu.mx

Paula Bonet-Meliá — bonet.paula@gmail.com

Nadine Schubert — nadine_schubert@hotmail.com

Lázaro Marín-Guirao — lazaro.marin@ieo.csic.es

Raquel Muñiz-Salazar — ramusal@uabc.edu.mx

Alejandro Cabello-Pasini — acabello@uabc.edu.mx

Alejandra Ferreira-Arrieta — alejandra.ferreira@uabc.edu.mx

Jessica Anayansi García-Pantoja — anayansi.garcia@uabc.edu.mx

José Manuel Guzmán-Calderón — jmguzman@uabc.edu.mx

Gabriele Procaccini — gpro@szn.it

Guillermo Samperio-Ramos — guillermo.samperio@uabc.edu.mx

José Miguel Sandoval-Gil — jose.miguel.sandoval.gil@uabc.edu.mx

Data of submission: 12/11/2025

Word count (main text): 4880

Figures (main text): 6

Tables (main text): 2

Figures (supplementary material): 4

Tables (supplementary material): 5

Highlight:

Extreme marine heatwave disrupts photosynthesis, nitrogen metabolism, and carbon balance in the seagrass *Phyllospadix scouleri*, suggesting a narrow thermal safety margin in the face of ocean warming.

Abstract:

Marine heatwaves (MHWs) are intensifying under climate change, yet the physiological limits that constrain seagrass resilience remain poorly defined. We experimentally tested the responses of the surfgrass *Phyllospadix scouleri*, a foundation species of the Northeast Pacific coast, to simulated MHWs of contrasting intensity. In a 27-day mesocosm experiment, plants were exposed to fluctuating temperatures representing a severe MHW (23.5 ± 1.5 °C) and an extreme MHW (26.5 ± 1.5 °C), while photosynthetic performance, respiration, nitrogen metabolism, oxidative stress, and growth were monitored during and after warming. *Phyllospadix scouleri* maintained photosynthetic capacity and carbon balance under severe warming but exhibited pronounced physiological disruption at extreme temperatures, including sustained photoinhibition, reduced nitrate assimilation, elevated respiration, and negative daily productivity. These effects persisted after heat stress, leading to reduced growth and indicating incomplete recovery. Multivariate analyses revealed a distinct transition from tolerance to functional breakdown near 26.5 °C, suggesting a physiological tipping point only 5–6 °C above current summer maxima in the area of the studied population. Our findings demonstrate that intensifying MHWs may rapidly erode the thermal safety margin of temperate seagrasses, pushing foundational coastal ecosystems toward metabolic instability and potential regime shifts under continued ocean warming.

Keywords:

Climate change, Marine heatwave, *Phyllospadix scouleri*, Physiology, Seagrass, Thermal safety margin, Thermal tolerance.

Abbreviations:

α: Photosynthetic efficiency, DP: Daily productivity, E_c: Compensation irradiance, E_k: Saturation irradiance, ETR: Electron transport rate, F_0: Minimum fluorescence, F_m: Maximum fluorescence, F_v/F_m: Maximum quantum yield, Gross-P_{max}: Gross maximum photosynthetic rate, MHW: Marine heatwave, Net-P_{max}: Net maximum photosynthetic rate, NPQ: Non-photochemical quenching, NRA: Nitrate reductase activity, NSC: Non-structural carbohydrates, R: Respiration rate, RGR: Relative growth rate; Φ_{PSII}: Effective quantum yield.

1. Introduction

Seagrass meadows are declining globally at alarming rates due to growing pressures from climate change and human activities (Dunic *et al*., 2021). As foundation species, their degradation implies the loss of entire ecosystems, with far-reaching ecological, socio-economic, and cultural consequences that threaten fisheries, shoreline stability, blue-carbon storage, and multiple societal values (Unsworth *et al*., 2022, Foster *et al*., 2025). Among the most severe disturbances affecting seagrass meadows is ocean warming, which is expected to drive a global spatial redistribution of seagrass species (Gouvêa *et al*., 2024). Closely associated with this long-term trend are marine heatwaves (MHWs), defined as discrete periods of anomalously high sea surface temperature relative to the local climatology (Hobday *et al*., 2016), which can trigger large-scale degradation and even mass mortality events in seagrass meadows (e.g., Marbà & Duarte 2010, Strydom *et al*., 2020).

Current knowledge on seagrass thermal physiology spans many species worldwide, yet remains dominated by studies on temperate taxa such as *Posidonia oceanica*, *Zostera marina*, and *Cymodocea nodosa* (Table S1). These experiments have tested warming scenarios ranging from +2 to +20 °C above local climatology and lasting from a few hours to several months. Although many exceed realistic MHW conditions, they consistently show that elevated temperatures reduce photosynthetic efficiency, deplete photosynthetic pigments, and increase oxidative stress, leading to reductions in growth, biomass, and shoot density. When thermal thresholds are surpassed, it results in irreversible tissue damage, necrosis, and mortality. Altogether, this evidence demonstrates the nonlinear thermal sensitivity of seagrasses, with sharp declines beyond species-specific limits.

These temperature-induced impacts arise from the disruption of fundamental physiological processes, including photosynthesis, oxidative balance, and carbon allocation (Nguyen *et al*., 2021). The tolerance of seagrasses to elevated temperatures is modulated by intrinsic biological attributes at both species and population levels, such as acclimative plasticity and adaptive capacity (Pazzaglia *et al*., 2021). Moreover, thermal tolerance can be further influenced by factors such as local adaptation, seasonal timing, plant ontogeny, and tissue age (Ruocco *et al*., 2019; Beca-Carretero *et al*., 2021; Entrambasaguas *et al*., 2021; Rinaldi *et al*., 2023). Evaluating thermal sensitivity across populations and temperature gradients is

129 therefore essential to refine forecasts of seagrass vulnerability under future climate scenarios
130 (Bennett *et al*., 2019; Starko *et al*., 2024).

131 Seagrass responses to warming also depend largely on the characteristics of each MHW,
132 particularly its intensity, duration, and frequency. Moderate temperature increases may
133 transiently stimulate metabolic processes such as photosynthesis (Beca-Carretero *et al*.,
134 2018), whereas more intense or prolonged events exceed species' thermal limits, causing
135 oxidative stress, reduced growth, and mortality (Collier & Waycott, 2014). As climate change
136 progresses, MHWs are becoming more frequent, longer lasting, and more intense, with
137 "extreme" events - once rare - projected to represent up to 70% of all occurrences by 2100
138 (Oliver *et al*., 2019). To better anticipate their ecological consequences, it is increasingly
139 important to assess seagrass responses across warming levels and under temperature regimes
140 that mimic, as closely as possible, real MHW conditions, encompassing both contemporary
141 events and projected future scenarios (e.g., Saha *et al*., 2020; Stipcich *et al*., 2022a; Gillis *et*
142 *al*., 2025).

143 Along the Northeast Pacific, and particularly on the coasts of the United States and Baja
144 California (Mexico), the frequency and intensity of MHWs have increased markedly in recent
145 decades (Bond *et al*., 2015; Wei *et al*., 2021). These extreme events have triggered
146 widespread ecological disruptions, including persistent declines in macrophyte assemblages
147 such as giant kelp forests (*Macrocystis pyrifera*; Arafeh-Dalmau *et al*., 2019; Beas-Luna *et*
148 *al*., 2020) and associated shifts in community structure. While much attention has been
149 focused on canopy-forming kelps, other neighboring coastal primary producers may be
150 equally vulnerable to increasing ocean temperatures.

151 Surfgrasses (*Phyllospadix scouleri* W.J. Hooker and *Phyllospadix torreyi* S. Watson) are key
152 foundation species that dominate the intertidal and shallow-subtidal rocky shores of the
153 Northeast Pacific, from Vancouver Island (Canada) to Baja California (Mexico) (den Hartog
154 & Kuo, 2006). Their high productivity (> 8000 g DW m^{-2} yr^{-1}; Ramírez-García *et al*., 1998)
155 and dense canopies (8000–12000 shoots m^{-2}; García-Pantoja *et al*., 2020) create structurally
156 complex habitats that support diverse assemblages of invertebrates and fish. With leaves that
157 can exceed 2 m in length, surfgrass meadows modulate physical, chemical, and biological
158 processes across intertidal pools and shallow (~10 m) rocky bottoms (Tharaldson, 2018;

159 Ruiz-Montoya *et al*., 2021). *Phyllospadix* meadows provide essential ecosystem services,
160 including coastal protection, nutrient cycling, carbon sequestration, and habitat provision
161 (García-Pantoja *et al*., 2020; Fields & Silbiger, 2022). Unlike most seagrasses, however,
162 surfgrasses thrive on wave-exposed rocky substrates, an adaptation made possible by their
163 specialized rhizome anchoring system (Cooper & McRoy, 1988), which enables them to
164 colonize high-energy coastal zones often inaccessible to other vascular plants.

165 Despite their ecological importance, surfgrasses remain among the least studied seagrass
166 groups worldwide (Strydom *et al*., 2023). Early work on *P. torreyi* identified an optimal
167 growth range of 12–14 °C and sharp declines above 17 °C, indicating a relatively narrow
168 thermal tolerance (Drysdale & Barbour, 1975). At lower latitudes, recent experiments
169 revealed that *P. torreyi* can transiently increase photosynthetic capacity under short-term heat
170 exposure (~25 °C for seven days), although this response coincides with carbon reserve
171 depletion, suggesting energetic trade-offs (Vivanco-Bercovich *et al*., 2022). In *P. scouleri*,
172 repeated exposures to warming (~24 °C) led to progressive declines in photosynthetic
173 efficiency, oxidative stress accumulation, and reduced nitrate uptake, despite temporary
174 maintenance of growth through carbon mobilization (Bonet-Melià *et al*., 2023; Vivanco-
175 Bercovich *et al*., 2024). Intertidal populations appear relatively tolerant to elevated
176 temperatures (Menge *et al*., 2020; Ruiz-Montoya *et al*., 2021), but recent findings indicate
177 that climate change is already shaping population structure and genetic diversity across
178 *Phyllospadix* species (Tavares *et al*., 2024). Collectively, these studies show that surfgrasses
179 can initially withstand moderate warming, but major uncertainties remain about the
180 physiological thresholds and resilience of *P. scouleri* under the extreme warming scenarios
181 projected for coming decades.

182 This study aimed to compare the physiological responses and growth of *P. scouleri* under
183 MHWs of different intensities, representing contemporary and future scenarios. We
184 conducted a 27-day mesocosm experiment in which subtidal adult plants were exposed to
185 two scenarios: (i) a severe MHW, with a maximum intensity of +5 °C, representing
186 contemporary events, and (ii) an extreme MHW, reaching +8 °C, simulating future
187 projections. Daily temperature fluctuations were incorporated in the experiment to resemble
188 natural conditions. Across two experimental phases (during heat exposure, and after warming

cessation), we analyzed a set of ecophysiological descriptors to identify acclimation mechanisms and physiological responses. These findings provide insights into the potential thermal thresholds of *P. scouleri*, offering a better understanding of its capacity to withstand climate-driven heat extremes, and supporting conservation strategies for these ecologically and functionally important coastal ecosystems.

2. Material and methods

2.1. Donor meadow and thermal history

The donor meadow is located on Todos Santos Island (31° 48' 25.66" N, 116° 47' 46.41" W), approximately 19 km offshore from Ensenada, Baja California, México, within the Pacific Islands Biosphere Reserve (Fig. 1A, B). This meadow spans over >32.000 m^2, extending from the intertidal to depths of ~ 7 m along a high energy, rocky coastline (Garcia-Pantoja *et al*., 2020). Seawater temperature in this region typically ranges between 15°C to 20°C, with peaks usually occurring in August - September (Fig. S1A). Yet, in the last few years, summer peak temperatures have repeatedly surpassed 23°C (Fig. S1B).

Historical satellite-derived sea surface temperature (SST) data indicate that this region has experienced over 100 marine heatwaves (MHWs) since 1982 (Marine Heatwave Tracker platform, www.marineheatwaves.org; Pixel: 116.875°W 31.875°N; Fixed baseline: 1982-2011). Most of these events lasted 10 days or less and were characterized by intensity anomalies ≤ 3°C, although a few reached intensities of up to 5.5 °C (Fig. S2). According to the classification framework proposed by Hobday *et al*. (2018), 88% of the events were categorized as "moderate", 18% as "strong", while only three were classified as "severe" and one as "extreme".

Submersible sensors (Onset-HOBO MX2202) were calibrated and anchored for two years within the donor meadow to obtain high-resolution, sub-daily thermal records beyond what is provided by daily mean satellite SST data. In situ temperature data from sensors showed high thermal variability at the donor meadow (Fig. S3). Discrepancies between satellite-derived and *in situ* measurements exceeded 3°C, with satellite SST underestimating maximum temperatures by ~2°C. For instance, *in situ* sensors recorded a peak of 24.3°C in August 2020, which was 1.7°C higher than satellite-derived values and nearly 4°C above the

climatological mean (Fig. 1C). This dataset was used to define the experimental temperature regimes, ensuring that treatments reproduced both the daily thermal variability and the magnitude of MHWs observed in the field.

2.2. Plant collection and acclimation

Phyllospadix scouleri plants were collected in September 2021 by divers from the subtidal zone (~5 m below mean sea level) of the donor meadow. Subtidal plants were selected over intertidal individuals because they are typically exposed to less extreme temperatures and less pronounced daily temperature fluctuations (Ruiz-Montoya *et al.*, 2021), and therefore likely represent the portion of the meadow most sensitive to MHWs. To preserve clonal integrity, plants were carefully detached from the rocks while maintaining ramet connections. Samples were transported in coolers within 2 hours to the Instituto de Investigaciones Oceanológicas (IIO) at the Universidad Autónoma de Baja California (UABC). To characterize field physiological conditions prior to acclimation, photobiological descriptors were measured immediately after collection, and leaf tissues were frozen at -80°C for subsequent biological analyses (Table S2).

Plants were acclimated for five days in an outdoor experimental system at a seawater temperature of 18.5 ± 1.5°C, consistent with the thermal regime recorded during the three weeks preceding collection (Fig. 1C). This system consisted of 12 independent tanks (1000 L), each serving as an experimental unit (EU). Each EU contained 6-8 shoot clumps (with ~200 connected shoots each), which were secured to rocks at the bottom of the tanks. To replicate natural light conditions at the collection site, neutral shading screens were used in order to maintain a maximum light intensity of ~200 µmol photon m^{-2} s^{-1} at midday, and a daily PAR dose of approximately 4.5 mol photon m^{-2} day^{-1}. Photosynthetically active radiation (PAR) and seawater temperature were monitored during the experiment both in the field and in the tanks using submersible data loggers (Onset HOBO MX2202) (Fig. 1D).

2.3. Thermal treatments: rationale and experimental setup

The experiment consisted of three temperature treatments: a control (18.5 °C), a severe-MHW (23.5 °C), and an extreme-MHW (26.5 °C) (Fig. 1D). Daily fluctuations of ± 1.5 °C were applied across all treatments to mimic natural diel variability recorded *in situ* (Fig. S3). The control was set to match the temperature recorded at the meadow at the time of sampling,

248 approximately 1 ºC below the climatological temperature for that time of year (i.e., 19.5 ºC,
249 Fig. 1D).

250 The severe-MHW treatment (with peaks of 25 °C) represents a realistic contemporary
251 anomalous event based on recent summer observations (Fig. S2). The extreme-MHW
252 treatment was designed to simulate a plausible upper-bound scenario under end-of-century
253 warming. According to the IPCC (2021), sea surface temperatures in the North Pacific are
254 expected to increase by approximately 3 °C by 2100 under high-emission scenarios (SSP5-
255 8.5). Furthermore, MHWs are expected to become more intense as baseline temperatures rise
256 and ocean–atmosphere feedbacks amplify thermal anomalies (Frölicher *et al*., 2018; Oliver
257 *et al*., 2019; Cael *et al*., 2024; Athanase *et al*., 2024). Combined with local sub-daily
258 variability, these projections suggest that short-term temperature extremes in the range of
259 26.5 ± 1.5 °C are increasingly to occur in upcoming decades. The classification of the
260 simulated MHWs followed the criteria proposed by Hobday *et al*. (2018), which define
261 intensity levels based on peak temperature anomalies relative to local climatology.

262 Each MHW treatment lasted seven days at peak temperature, flanked by two-day warming
263 and cooling transitions (Fig. 1D). During these transitions, the temperature increased or
264 decreased at rates of ~2 °C day^{-1} for the severe-MHW and ~4 °C day^{-1} for the extreme-MHW,
265 values within the range of daily variation recorded by in situ sensors at the study site.
266 Following the heatwave period, all plants underwent a 7-day post-warming phase at control
267 temperature (18.5 ± 1.5 °C), identical to that at the control treatment. Physiological responses
268 were assessed at two time points: at the conclusion of the heatwave period (warming phase)
269 and seven days after temperatures returned to control levels (post-warming phase).

270 Within the mesocosm facility, temperature was regulated using chillers (Aqua Logic Multi-
271 temp Chiller MT-4, 3HP) and submersible heaters. A water pump (AQUAPAK SUPRA
272 15/1230, flow rate: 100-390 L/min) was utilized to recirculate seawater between reservoir
273 tanks and the four EUs of each treatment. Aeration was supplied from the bottom of each
274 tank to ensure vertical mixing and water column homogenization. Partial seawater
275 replacements were made during the experiment to maintain water quality. Salinity was kept
276 at 33.4 ± 0.3. Distilled water was added daily to offset the loss of water through evaporation.

2.4. Physiological traits and growth

At the end of the two experimental phases, random shoots were collected from the EUs for physiological analysis and growth measurements. For each physiological trait, measurements from two samples per EU were averaged to obtain an accurate experimental replicate (n = 4 per treatment), except for photosynthesis-irradiance (P-E) curves, which were conducted on a single sample per EU. The same number of replicates was utilized for the initial condition characterization. To standardize the measurements, all samples were taken from the middle section of the second mature leaf.

2.4.1. Photosynthesis and Respiration (P vs. E curves)

Photosynthetic and respiratory rates were measured in leaf segments using a custom-made incubation setup, consisting of 200 mL borosilicate jacketed chambers maintained at controlled temperatures via a circulating bath and illuminated by four 10W LED light sources, all regulated through customized software. Magnetic stirrers ensured water homogenization during incubations.

Oxygen evolution was measured using optodes (Dipping Probe DP-PSt3, PreSens, Germany) connected to a fiber-optic oxygen meter (OXY4 SMA, PreSens, Germany), with data acquisition controlled via Measurement Studio 2 software (PreSens, Germany). To ensure accurate photosynthetic measurements and prevent underestimation due to oxygen oversaturation or carbon limitation, a biomass-to-seawater volume ratio of 0.03–0.05 g DW L^{-1} was maintained.

Leaf segments (~3 cm^{2}) were initially incubated in darkness for 10 min to determine respiration (R) and then exposed to increasing PAR irradiance levels (0–801 µmol photons m^{-2} s^{-1}) for 5 min at each intensity step. Light intensities were calibrated using a spherical (4π) quantum sensor (Biospherical Instruments, California, USA).

The maximum net photosynthetic rate (net-P_{max}; µmol O_2 g^{-1} DW h^{-1}) was determined by averaging the maximum values above the saturating irradiance (E_k = net-P_{max}/ α; µmol photon m^{-2} s^{-1}). The gross maximum photosynthetic rate (gross-P_{max}; µmol O_2 g^{-1} DW h^{-1}) was calculated as net-P_{max} + R. Photosynthetic efficiency (α) was calculated as the slope of the regression line fitted to the initial linear portion of the P vs. E curve. The compensation

irradiance (E_c; µmol photon m^{-2} s^{-1}) was determined as the X-axis intercept of this linear portion (Fig. S4).

2.4.2. Chlorophyll a fluorescence and absorptance

Chlorophyll *a* fluorescence from PSII was measured using a portable Diving-PAM fluorometer (Walz, Germany). Leaves were carefully cleaned of epiphytes and positioned in the DCL-8 leaf-clip holder to ensure a fixed distance between the tissue and the fiber optic sensor. Maximum quantum yield (F_v/F_m), basal fluorescence (F_o), and maximum fluorescence (F_m) were recorded from plants kept in darkness overnight, while effective quantum yield (Φ_{PSII}), F_o', and F_m' were measured in light-acclimated plants exposed to actinic light (60 s, 247 µmol photon m^{-2} s^{-1}). Dark and light adapted measurements were taken at the same leaf portion.

Absolute electron transport rate (ETR) was calculated using:

$$ETR = \Phi_{PSII} \times 247 \times A \times 0.5$$

where A represents leaf absorptance (see below), 247 is the actinic light intensity, and 0.5 accounts for the assumption that half of the incident photons pass through PSII (Beer *et al*., 2014).

Leaf absorptance (A) was determined as:

$$A = 1 - (LT / L0) – TW$$

where LT is the transmitted light through the tissue, L0 is the total incident light emitted by the lamp, and TW is the transmitted light through a bleached leaf (2% bleach for 24 hours). Light transmission was measured using a miniature fiber optics quantum sensor (Diving-F1, Walz, Germany) integrated into the Diving-PAM fluorometer (Walz, Germany). The light sensor was secured in the leaf clip to maintain a consistent geometry between the leaf, lamp, and sensor.

Finally, non-photochemical quenching (NPQ) was calculated as:

$$NPQ = (F_m - F_{m'})/F_{m'}$$

where F_m is the maximum fluorescence in dark-adapted plants, and F_m' is the fluorescence recorded under actinic light exposure.

2.4.3. Pigment content

Leaf pigments were extracted from ~15 mg fresh weight (FW) of homogenized leaf tissue using 100% acetone, with $MgCO_3$ added to prevent acidification (Dennison, 1990). Extracts were stored at 4°C in darkness for 24 hours. After centrifugation (1000 × g, 10 min), absorbance was measured at 470, 646, and 663 nm using a spectrophotometer and 1 mL cuvettes. Chlorophyll *a* (Chl *a*), chlorophyll *b* (Chl *b*), and total carotenoid concentrations were calculated using the equations of Lichtenthaler & Wellburn (1983) and expressed as mg g^{-1} FW.

2.4.4. Total phenolic content, antioxidant capacity and lipid peroxidation

Phenolic and antioxidant compounds were extracted from dried, ground leaf tissue (0.02 g DW) using 1 mL of 80% methanol. Samples were incubated in darkness for 24 hours and then centrifuged at 10,000 rpm for 10 minutes. The resulting extracts were used to quantify total phenolic content and antioxidant capacity.

Total phenolic content was determined using a modified Folin–Ciocalteu assay with gallic acid as the standard (Singleton & Rossi, 1965). A 0.01 mL aliquot of the methanolic extract was diluted in 1 mL of distilled water (dH_2O), followed by the addition of 0.1 mL Folin–Ciocalteu reagent and 0.3 mL Na_2CO_3-saturated dH_2O. The mixture was homogenized, heated at 40°C for 3 minutes, and absorbance was measured at 765 nm using a spectrophotometer. Total phenolic content was expressed as gallic acid equivalents (mg Eq. GA g^{-1} DW).

Radical scavenging activity was quantified from the same methanolic extracts following Sabeena-Farvin & Jacobsen (2013). The reaction mixture was prepared by mixing 0.1 mL of a 1:10 diluted extract (in 80% methanol) with 1 mL of 60 µM 2,2-diphenyl-1-picrylhydrazyl (DPPH) dissolved in 90% methanol. Absorbance was recorded at 517 nm after 30 minutes of DPPH addition. Total antioxidant capacity was expressed as ascorbic acid equivalents (mg Eq. AA g^{-1} DW).

Oxidative damage was determined by quantifying malondialdehyde (MDA). Lipid peroxidation was quantified using the thiobarbituric acid-reactive substances (TBARS) assay, following Hodges *et al*. (1999) and Correia *et al*. (2006). Frozen leaf tissue (0.2 g FW) was subjected to mechanical grinding in 2 mL of 80% ethanol. The homogenate was centrifuged (10 min, 3000 × g, 4°C), and the supernatant was mixed with 20% trichloroacetic acid (TCA) and 0.5% thiobarbituric acid (TBA). Blanks were prepared by mixing the supernatant with 20% TCA. Samples were incubated at 90°C for 30 minutes and centrifuged again (3000 × g, 10 min). Absorbance of the extracted supernatants was measured at 440, 532, and 600 nm using a spectrophotometer. Lipid peroxidation was expressed as malondialdehyde equivalents (Eq. MDA) using a molar extinction coefficient of 155 mM^{-1} cm^{-1}, according to Hodges *et al*. (1999).

2.4.5. Nitrogen uptake and nitrate reductase activity

Nitrogen uptake was quantified by incubating shoots in artificial seawater enriched with 5 µM of isotopically labeled nitrate ($K^{15}NO_3$, 99 atom % ^{15}N; Cambridge Isotope Laboratories) for 30 minutes. This concentration is similar to nitrate levels observed in surfgrass meadows during upwelling events, which tend to be most intense and frequent in the region throughout the spring and summer (Espinosa-Carreón *et al*., 2001). Incubations were conducted in separate plastic bags (2 L, n = 3), which were sealed and left floating during the incubation period inside the experimental tanks, ensuring that temperature and irradiance matched those of the respective treatment. Each incubation encompassed eight randomly selected shoots per tank and treatment, maintaining a weight-to-volume ratio of ~4.5 g FW L^{-1}. To preserve vegetative integrity, a small rhizome segment (~1 cm) was retained in each shoot. Nitrogen uptake rates were calculated using the equations of Sandoval-Gil *et al*. (2016). Dried and ground leaf tissues were analyzed for ^{15}N enrichment and total nitrogen content (N-content) at the University of California Davis-Stable Isotope Facility, using an elemental analyzer interfaced with a continuous-flow isotope ratio mass spectrometer (IRMS). To assess nitrogen assimilation, nitrate reductase (NRA) activity was measured *in vivo* from leaf segments of three shoots per tank and treatment, following Alexandre *et al*. (2004), using leaves distinct from those analyzed for nitrate uptake.

2.4.6. Non-structural carbohydrates

Total soluble non-structural carbohydrates (NSCs), including free sugars and starch, were quantified using the colorimetric phenol-sulfuric acid method (Dubois *et al*., 1956), with glucose as the standard. Leaf tissues were oven-dried at 60°C to a constant weight, then ground into a fine powder. The powdered tissue was digested in 0.1 N HCl (60°C, 3 h), centrifuged (4000 × g, 5 min), and the supernatant was mixed with 3% phenol and concentrated sulfuric acid. Absorbance was recorded at 490 nm using a spectrophotometer. NSC content was expressed as mg g^{-1} DW.

2.4.7. Daily Productivity

Daily productivity (DP; µmol O_2 g^{-1} DW day^{-1}) was estimated by integrating the P vs. E response curves with the averaged diurnal irradiance cycle recorded in the experimental system. Unlike methods that rely on fixed photosynthetic efficiency (α) and net-P_{max}, we applied polynomial functions (3rd or 4th degree) fitted to the P vs. E data from each experimental unit (EU, n = 4), with the y-intercept fixed at R.

Diurnal irradiance was recorded using Onset HOBO MX2202 sensors (n = 3) placed at mid-water depth to capture both direct and reflected sunlight within the aquaria. Light intensity (Lux) was converted to photons m^{-2} s^{-1} using a conversion factor of 0.0185. Each recorded irradiance value was entered into the polynomial equation to estimate instantaneous photosynthetic rates. Integrating these rates over the whole daylight period yielded cumulative daily productivity.

2.4.8. Relative leaf growth rate

All leaves of each shoot were marked just above the sheath at the beginning of both the warming and post-warming phases using the hole punch method adapted from Zieman (1974). At the end of each experimental phase, all marked shoots were harvested, and newly formed leaf tissue (i.e., below the mark) was dried and weighed for each shoot. Shoot growth was expressed as relative leaf growth rate (RGR; mg g^{-1} DW day^{-1}), calculated with respect to total shoot biomass.

2.5. Statistical analysis

2.5.1. Univariate analysis

All statistical analyses were conducted in R (R Core Team, 2020), with a significance level of $\alpha = 0.05$. Prior to hypothesis testing, data normality was assessed using the Shapiro-Wilk test, and homogeneity of variances was evaluated using Bartlett's test (package car). Variables that deviated from normality were log-transformed to improve distribution symmetry (e.g., chl *b* content and nitrate uptake rate). A two-way ANOVA was performed to assess the main and interactive effects of treatment (three levels: control, severe-MHW and extreme-MHW) and experimental phase (two levels: warming phase and post-warming phase) on all measured physiological descriptors. A standard type III ANOVA was used for the variables that met the parametric assumptions. For heteroscedastic variables (e.g., F_m, and NRA activity), ANOVA models were adjusted using White's correction to account for variance heterogeneity. Tukey's HSD post-hoc test was applied when significant differences were detected to compare means among treatments and time points. The non-parametric Games-Howell test was used for *post-hoc* comparisons in heteroscedastic variables.

2.5.2. Multivariate analysis

Principal Component Analysis (PCA) was performed using the *prcomp* function in R on a correlation matrix (scale. = TRUE). The number of components retained was based on the Kaiser criterion (eigenvalue > 1). Loadings were used to identify key variables contributing to each axis, and scores were used to visualize sample distribution across treatments and time points. To reduce redundancy and improve the interpretability of the PCA, a variable selection approach was applied prior to the analysis. Firstly, variables that were mathematically derived from others were excluded to prevent artificial correlations and overrepresentation of specific physiological processes. Secondly, variables that did not exhibit significant responses to treatments in the univariate analysis were removed. Lastly, correlated variables that reflected similar but independently measured physiological processes were combined into composite indices (Table S3). Variables were standardized (z-score), and grouped indices were averaged prior to analysis.

Multivariate differences were also tested using Permutational ANOVA (PERMANOVA, *adonis2* function, *vegan* package) based on a Euclidean distance matrix. Treatment,

446 experimental Phase, and their interaction were included as fixed factors, with 999
447 permutations. Pairwise comparisons among Treatment × Experimental Phase combinations
448 were also performed.

449 3. Results

450 3.1. Photosynthesis and respiration

451 Photosynthetic capacity varied across treatments and experimental phases, with significant
452 treatment effects detected for net-P_{max}, E_k, E_c and R (Table 1). The most pronounced changes
453 occurred under the extreme-MHW treatment, where net-P_{max} and E_k decreased by 12% and
454 22%, respectively, during the warming phase, and by 39% and 19% during the post-warming
455 phase, relative to the control plants (Figs. 2A, C). These reductions were accompanied by
456 significant increases in R, which rose by 77% during the warming phase and by 113% post-
457 warming (Fig. 2F). Similarly, E_c increased by 53% during warming and by 181% during
458 post-warming under extreme-MHW conditions (Fig. 2E). In contrast, no significant
459 treatment effects were detected for gross-P_{max} or α (Figs. 2B, D).

460 3.2. Chlorophyll *a* fluorescence and absorptance

461 The photochemical performance of photosystem II was significantly affected by warming,
462 as evidenced by a decline in the maximum photochemical efficiency (F_v/F_m) in plants
463 exposed to the extreme-MHW treatment (Table 1). Compared to the control, F_v/F_m decreased
464 by 3% during the warming phase and by 7% in the post-warming phase (Fig. 3A).

465 The effective quantum yield (Φ_{PSII}) showed a significant interaction between treatments and
466 experimental phase (Table 1). The highest Φ_{PSII} was observed in plants subjected to the
467 severe-MHW treatment during the warming phase, significantly exceeding values in both the
468 control and extreme-MHW groups. By the post-warming phase, Φ_{PSII} had declined in both
469 MHW treatments, with the extreme-MHW group exhibiting the steepest drop, 21% lower
470 than the control (Fig. 3B).

471 The electron transport rate (ETR) followed a pattern similar to that of Φ_{PSII}, showing a
472 significant interaction between treatment and experimental phase (Table 1). During the
473 warming phase, ETR was highest in the severe-MHW treatment, approximately 21% higher

than the control. In contrast, ETR declined sharply in the extreme-MHW group during the post-warming phase, reaching values 30% lower than the control (Fig. 3C).

Basal fluorescence (F_0) was not significantly affected by experimental phase, treatment, or their interaction (Table 1). However, an increasing trend was observed during the warming phase across both MHW groups (Fig. 3D). By the post-warming phase, F_0 values remained higher only in the extreme-MHW treatment.

In contrast, maximum fluorescence (F_m) was significantly influenced by experimental phase, treatment, and their interaction (Table 1). During the warming phase, plants in the severe-MHW treatment exhibited the highest F_m values. By the post-warming phase, F_m declined in all treatments (Fig. 3E).

Non-photochemical quenching was lowest in control plants during the warming phase (Fig. 3F). Due to inconsistencies in measurements, control values during the post-warming phase were excluded from the analysis. Both MHW treatments showed increased NPQ levels, but only the extreme-MHW group was significantly higher than the control (Table 1). NPQ peaked during the warming phase in this treatment, reaching values 106% higher than the control.

3.3. Pigment content

Pigments contents were not significantly affected by the experimental treatments. However, for carotenoids, pigment levels varied between experimental phases (Tables 1, 2). Plants in the severe-MHW treatment showed the highest carotenoid concentrations during the warming phase, while those in the extreme-MHW treatment reached their peak values during the post-warming phase. These differences, however, were not statistically significant.

3.4. Total phenolic content, antioxidant activity and lipid peroxidation

Leaf phenolic content was significantly reduced in plants exposed to warming (Table 1). Plants in the severe-MHW and extreme-MHW treatments exhibited reductions of approximately 27% and 21%, respectively, during the warming phase compared to the control (Table 2). By the post-warming phase, the phenolic content increased in both treatments but remained 5% lower in severe-MHW and 17% lower in extreme-MHW plants compared to control levels.

Total antioxidant capacity was also significantly affected by treatment (Table 1). During the warming phase, both severe-MHW and extreme-MHW plants exhibited approximately 40% lower antioxidant capacity than control plants (Table 2). However, only the extreme-MHW group differed significantly from the control. By the post-warming phase, severe-MHW plants recovered to control levels, while values in the extreme-MHW group remained 30% lower than those of the control.

Lipid peroxidation was significantly affected by treatment, with a significant interaction with experimental phase (Table 1). In the severe-MHW treatment, lipid peroxidation showed a significant decrease during the warming phase, reaching values 31% lower than the control, but returned to near-control levels by the post-warming phase (Table 2). In contrast, lipid peroxidation in extreme-MHW plants did not vary significantly.

3.5. Nitrogen uptake and NRA

Nitrate uptake was significantly affected by the interaction between treatment and experimental phase (Table 1). During the warming phase, plants in the extreme-MHW treatment exhibited the highest uptake rates, while in the severe-MHW group uptake was 38% lower than in the control (Fig. 4A). By the post-warming phase, severe-MHW and extreme-MHW plants exhibited contrasting responses, but both had showed higher uptake rates than the control, increasing by 82% and 43%, respectively.

Nitrate reductase activity (NRA) was also significantly affected by the interaction between treatment and experimental phase (Table 1). During the warming phase, control plants showed a modest 16% reduction in NRA compared to initial conditions. In comparison, severe-MHW and extreme-MHW plants exhibited sharp declines of 71% and 97%, respectively, relative to the control (Fig. 4B). By the post-warming phase, NRA continued to decline in control plants, remained stable in the severe-MHW group, and showed a drastic increase in the extreme-MHW treatment, reaching values 438% higher than those of the control.

3.6. Carbohydrates, productivity and growth

Leaf non-structural carbohydrate (NSC) content did not vary significantly across treatments (Table 1), although plants in the severe-MHW treatment exhibited a 52% increase in NSC content relative to the control (Fig. 5A).

Daily productivity (DP) was significantly influenced by treatment (Fig. 5B). Control plants experienced a substantial 58% decline in DP during the warming phase compared to initial conditions. Plants in the severe-MHW treatment showed slightly lower DP than the control, although the difference was not statistically significant. In contrast, the extreme-MHW treatment resulted in significantly lower DP values compared to both the control and severe-MHW, with negative productivity observed during both the warming and post-warming phases.

Leaf relative growth rate (RGR) was strongly affected by treatment (Fig. 5C). control and severe-MHW plants maintained similar RGR values throughout the experiment. In contrast, plants exposed to the extreme-MHW treatment showed a 45% reduction during the warming phase and a 62% reduction during the post-warming phase compared to the control.

3.7. Multivariate results

Principal Component Analysis (PCA) revealed clear patterns of multivariate physiological variation across treatments and experimental phases (Fig. 6). The first three principal components explained 78.2% of the total variance, with PC1 (31.8%) and PC2 (24.4%) accounting for the greatest proportion (Table S4). Samples from the extreme-MHW treatment, particularly during the post-warming phase, were clearly separated from those of the control and severe-MHW groups along PC1. This separation was driven by decreases in respiration, nitrogen assimilation, and carotenoids, whereas control and severe-MHW samples expressed higher values of leaf growth and photosynthesis. PC2 further distinguished extreme-MHW samples during the warming phase, which were associated with increased nitrate uptake and respiration. PC3 (22.0%) captured additional variation related to antioxidant capacity and oxidative stress, contributing to the separation of samples within the control and severe-MHW treatments during the post-warming phase.

PERMANOVA confirmed significant effects of treatment (R^2 = 0.33, P = 0.001), experimental phase (R^2 = 0.15, P = 0.001), and their interaction (R^2 = 0.23, P = 0.001) on multivariate physiological profiles (Table S5). Pairwise comparisons revealed that the extreme-MHW treatment differed significantly from both the control and severe-MHW treatments during both the warming and post-warming phases, consistent with the separation observed in the PCA. The severe-MHW group differed from the control during the warming

563 phase but not during the post-warming phase, suggesting partial recovery or convergence
564 toward baseline conditions by the end of the experiment.

565 4. Discussion

566 As marine heatwaves (MHWs) intensify under climate change, foundation species such as
567 seagrasses are being pushed toward their physiological limits, threatening the resilience of
568 the coastal ecosystems they support. This study examines how the surfgrass *Phyllospadix*
569 *scouleri* responds physiologically to increasing thermal stress, revealing the upper limits of
570 its thermal tolerance (Fig. 7). While *P. scouleri* maintained physiological stability under a
571 severe MHW (T_{mean} = 23.5 °C, T_{max} = 25 °C), exposure to an extreme MHW (T_{mean} = 26.5
572 °C, T_{max} = 28 °C) caused pronounced photosynthetic impairment, supression of nitrogen
573 assimilation, elevated respiration and a negative carbon balance, ultimately leading to
574 reduced leaf growth. These findings indicate that future, more intense MHWs could exceed
575 the thermal tolerance of surfgrass populations, potentially threatening their ecological
576 functioning and long-term persistence.

577 4.1. Mechanisms of Physiological Tolerance vs. Breakdown

578 Exposure to a severe MHW did not negatively affect the photosynthetic performance of *P.*
579 *scouleri*. Both net- and gross-P_{max} remained stable, and the functionality of the
580 photosynthetic apparatus at thylakoid level (i.e., ETR and Φ_{PSII}) was even enhanced,
581 indicating that the species' thermal tolerance (at least at photosynthetic metabolism level)
582 was not surpassed. Moderate warming has also been shown to increase photosynthesis in *P.*
583 *torreyi* (Vivanco-Bercovich *et al*., 2022) and other species (Beca-Carretero *et al*., 2018;
584 Lawrence & Bolton, 2022), likely due to enhanced enzyme activity and protein mobility in
585 the thylakoid membrane.

586 In contrast, exposure to the extreme MHW appeared to push *P. scouleri* beyond a
587 physiological threshold, resulting in marked declines in its photosynthetic performance,
588 including reductions in net-P_{max}, gross-P_{max}, E_k, F_v/F_m, Φ_{PSII}, and ETR. Photosynthetic
589 alterations in seagrasses under heat stress are well documented (e.g., Costa *et al*., 2021;
590 Nguyen *et al*., 2021; Deguette *et al*., 2022), and are often linked to damage in key components
591 of PSII, such as light-harvesting complexes, reaction centers, and oxygen-evolving

592 complexes (Mathur *et al*., 2014). As chlorophyll *a* and *b* levels remained stable, it is likely
593 that functional damage to thylakoid membranes was the main cause of photosynthetic
594 inhibition (Marín-Guirao *et al*., 2018). The observed decrease in F_v/F_m, along with increased
595 basal fluorescence (F_0), further supports stress to PSII structure (Allakhverdiev *et al*., 2008).

596 Our results showed that non-photochemical quenching (NPQ) increased in *P. scouleri*
597 exposed to the extreme MHW during both experimental phases. This enhancement reflects
598 the activation of a photoprotective mechanism that dissipates excess light energy as heat
599 through the xanthophyll cycle, thereby preventing de production of reactive oxygen species
600 and oxidative stress (Ruocco *et al*., 2019; Murchie & Ruban, 2020; Vivanco-Bercovich *et*
601 *al*., 2024). Notably, no increase in lipid peroxidation was detected, suggesting either absence
602 of oxidative damage to membranes or sufficient antioxidant capacity to counteract stress
603 (Gururani *et al*., 2015). Likewise, total antioxidant capacity and phenolic content remained
604 unchanged, indicating marginal stimulation of antioxidant defenses under warm conditions.

605 Warming also affected nitrogen metabolism in *P. scouleri*, but responses varied with MHW
606 intensity. As temperature increased NRA declined, consistent with earlier reports (Bonet-
607 Melià *et al*., 2023). However, contrary to expectations, nitrate uptake decreased under severe
608 warming but increased under extreme conditions. This pattern may reflect complex
609 interactions among nitrogen incorporation, assimilation, translocation, and storage
610 investment and mobilization processes (Touchette & Burkholder, 2007; Alexandre *et al*.,
611 2010), though these mechanisms remain to be fully explored. Under extreme MHW, high
612 uptake rates coupled with low assimilation suggest a compensatory strategy to maintain
613 internal nitrogen stores, as documented in seaweeds (Gordillo, 2012). Nevertheless, these
614 disruptions were transient, with both uptake and assimilation recovering, or even surpassing,
615 control levels once warming ceased.

616 These results demonstrate that when MHWs exceed a critical threshold, *P. scouleri*
617 undergoes a disruption in carbon balance atributable to a mismatch between photosynthetic
618 production and respiratory demand. While moderate warming (~25–26 °C) was tolerated
619 without excessive respiratory demand (Vivanco-Bercovich *et al*., 2022; 2024), exposure to
620 the extreme MHW caused sustained elevation in R. Given the temperature sensitivity of
621 seagrass R (Marín-Guirao *et al*., 2016; Beca-Carretero *et al*., 2018), it is probable that this

pushed *P. scouleri* beyond a metabolic tipping point, leading to negative daily productivity. The observation that the NSC content of leaves remained stable suggests that plants relied on alternative carbon pools, most likely rhizome starch reserves, reflecting the flexible and spatially complex carbon economy of seagrasses (Marín-Guirao *et al*., 2018; Ruocco *et al*., 2021). Reduced leaf growth under extreme conditions may thus reflect an energy conservation strategy, prioritizing cellular maintenance and repair over biomass accumulation (Ruocco *et al*., 2019), a potential early indicator of long-term population decline.

This shift from tolerance to functional collapse was clearly captured in the multivariate analyses. The results of the PCA analysis revealed that *P. scouleri* plants exposed to the severe-MHW recovered to near-control physiological states following the cessation of warming (i.e. post-warming phase). At the same phase, plants subjected to the extreme-MHW remained clearly separated, driven by sustained R, impaired photosynthetic performance, reduced nitrate assimilation, and limited growth. These differences were further corroborated by the PERMANOVA. Respiration emerged as a key variable contributing to this divergence, illustrating how sustained energetic imbalance can cascade across physiological pathways and limit recovery capacity. Together, these findings highlight that while *P. scouleri* can recover from moderate thermal stress, exposure to extreme warming events may induce prolonged dysfunction that compromises its resilience.

4.2. Implications for Future Climate Change and Conclusions

Previous research has shown that exposure to 25°C can induce physiological alterations in *P. scouleri* without excerting a significant effect on productivity and growth (Vivanco-Bercovich *et al*., 2024). However, in this study, the extreme MHW scenario (T_{mean} = 26.5°C; T_{max} = 28°C) caused severe photosynthetic impairment, carbon imbalance, and growth suppression, suggesting a critical thermal threshold beyond which survival may be compromised. Taken together, the available evidence suggests that 26.5°C (as a daily average for at least seven days) may represent a tipping point (T_{lim}) for surfgrass thermal resistance in the northern Baja California Peninsula.

This threshold gains further significance when considered in the context of recent thermal trends in the region. The mean maximum summer temperature (T_{max}) in the study region was

~20.5°C between 1990 and 2019, rising to 21.5°C in the period 2014–2019. This suggests that the current thermal safety margin (TSM = T_{max} - T_{lim}) for *P. scouleri* populations in northern Baja California Peninsula is approximately 5 - 6°C. While this study focused on a local population, the physiological limit observed here aligns closely with the ~27.5 °C upper thermal limit reported for temperate seagrasses worldwide (Marbà *et al*., 2022), reinforcing its relevance for regional thermal vulnerability assessments.

Continued ocean warming and increasingly intense MHWs may significantly reduce this margin in the near future. Recent temperature records indicate that sea surface temperature in the study region has repeatedly exceeded 23°C, with MHW peaks reaching 25°C in recent years (Fig. S1B), approaching the estimated T_{lim} for *P. scouleri*. Mass mortality events have already been reported for seagrass populations with comparable TSMs across both temperate and tropical regions (Marbà & Duarte, 2010; Moore *et al*., 2014; Thomson *et al*., 2015; Carlson *et al*., 2018), suggesting that *P. scouleri* may likewise be vulnerable to future climate-driven warming events. This risk is further supported by biogeographic projections predicting range contractions and genetic erosion at the southern edge of *Phyllospadix* spp., including northern Baja California populations, under future warming scenarios (Tavares *et al*., 2024).

Further supporting this concern, global-scale projections indicate that climate change may result in widespread reductions of seagrass biomass of up to 9.25%, with significant losses expected in warm-temperate and tropical regions (Gouvêa *et al*., 2025). This observation suggests the possibility that the growth suppression observed in *P. scouleri* under extreme warming could foreshadow broader declines in seagrass meadows as marine heatwaves become more frequent and intense. Similar thermal thresholds have driven long-term productivity declines in *Posidonia oceanica* (Litsi-Mizan *et al*., 2023), exemplifying the potential consequences of carbon imbalance events in seagrass systems.

Such losses are not merely reductions in biomass, they represent a weakening of critical ecosystem functions. As foundational species, seagrasses play a central role in nutrient cycling, carbon sequestration, shoreline stabilization, and habitat provision for diverse marine communities (Unsworth *et al*., 2022). The disruption of nitrogen assimilation observed in *P. scouleri*, particularly the suppression of nitrate reductase activity (NRA)

682 during heatwaves, indicates that warming can compromise essential metabolic pathways that
683 sustain productivity and their role as effective biofilters in nutrient-enriched coastal waters
684 (Bonet-Melià *et al*., 2023). If MHWs continue to exceed physiological thresholds, the long-
685 term resilience of these ecosystems could be undermined. This evidences not only the
686 ecological vulnerability of surfgrass meadows, but also the urgent need to monitor key
687 physiological indicators such as nitrogen metabolism, respiration and growth, which can
688 signal early declines in the ecosystem services these habitats provide.

689 This study reveals *P. scouleri*'s vulnerability to temperatures representative of future MHWs.
690 However, the long-term persistence of this species is also contingent on seasonal and life-
691 stage variability in thermal tolerance (Beca-Carretero *et al*., 2021; Olsen *et al*., 2012;
692 Guerrero-Meseguer *et al*., 2017), and potential acclimation through stress memory
693 mechanisms (Nguyen *et al*., 2020; Pazzaglia *et al*., 2021, 2022; Stipcich *et al*., 2022b).
694 Moreover, thermal tolerance may differ among populations inhabiting environments with
695 contrasting temperature regimes, such as along depth gradients, where plants at shallower
696 sites are exposed to warmer and more fluctuating conditions (Marín-Guirao *et al*., 2016).
697 Conversely, additional stressors such as eutrophication, light reduction, and altered trophic
698 interactions may compound thermal impacts and further constrain *P. scouleri*'s resilience
699 (Hernán *et al*., 2017; Mvungi & Pillay, 2019; Vivanco-Bercovich *et al*., 2022; Pazzaglia *et*
700 *al*., 2022). These complex interactions complicate predictions of future seagrass persistence
701 and underscore the need for integrated, multi-stressor studies to better anticipate *P. scouleri*'s
702 resilience under climate change.

703 Moving forward, research should examine thermal vulnerability across seagrass life stages,
704 with particular attention given to germination and seedling development, which have been
705 found to be more sensitive to environmental stress (e.g., Rinaldi *et al* 2023). In the context
706 of surfgrasses, the broader impacts of MHWs on spatial distribution and long-term
707 persistence remain uncertain, raising questions about whether warm-edge populations exhibit
708 greater tolerance or heightened vulnerability (Bennet *et al*., 2022). Beyond plant-specific
709 traits, future studies should also address how additional MHW characteristics, including
710 duration, timing, and interval between events, shape physiological responses and recovery
711 trajectories. Expanding such work across species and bioregions will facilitate the

identification of generalizable thresholds of resilience and the differentiation of context-dependent responses.

Author contributions

M.V.B., P.B.M., and J.M.S.G. planned and designed the research. M.V.B., P.B.M., J.A.G.P., J.M.S.G., and J.M.G.C. conducted the fieldwork, experiments and collected the data. M.V.B. and A.F.A. performed the laboratory analyses with input from P.B.M. M.V.B. and J.M.S.G. analyzed data. M.V.B. led the writing of the manuscript with substantial contributions from all co-authors. All authors discussed the results and approved the final version of the manuscript.

Competing Interests

The authors declare no conflict of interest

Funding

This work was supported by the CONACYT-Ciencia Básica Project (A1-S-8382) granted to J.M. Sandoval-Gil. Doctoral CONACYT (Consejo Nacional de Ciencia y Tecnología) scholarships were awarded to P. Bonet-Melià and M. Vivanco-Bercovich. Additional support was provided by a Rufford Small Grant awarded to M. Vivanco-Bercovich. G. Procaccini was partially supported by the European Union - NextGenerationEU National Recovery and Resilience Plan (NRRP), Mission 4 Component 2 Investment 1.4, Project Code: CN00000033.

Data availability

All primary data supporting this study are prepared for deposition in Dryad and will be publicly available upon article acceptance. The dataset will include raw and processed physiological measurements, experimental temperature records, and statistical scripts.

References

Alexandre A, Silva J, Santos R. **2004**. The maximum nitrate reductase activity of the seagrass *Zostera noltii* (Hornem.) varies along its vertical distribution. *Journal of Experimental Marine Biology and Ecology* **307**: 127–135.

Alexandre A, Silva J, Santos R. **2010**. Inorganic nitrogen uptake and related enzymatic activity in the seagrass *Zostera noltii*. *Marine Ecology* **31**: 539–545.

Allakhverdiev SI, Kreslavski VD, Klimov VV, Los DA, Carpentier R, Mohanty P. **2008**. Heat stress: an overview of molecular responses in photosynthesis. *Photosynthesis Research* **98**: 541.

Arafeh-Dalmau N, Montaño-Moctezuma G, Martínez JA, Beas-Luna R, Schoeman DS, Torres-Moye G. **2019**. Extreme Marine Heatwaves Alter Kelp Forest Community Near Its Equatorward Distribution Limit. *Frontiers in Marine Science* **6**: 499.

Athanase M, Sánchez-Benítez A, Goessling HF, Pithan F, Jung T. **2024**. Projected amplification of summer marine heatwaves in a warming Northeast Pacific Ocean. *Communications Earth & Environment* **5**: 1–12.

Beas-Luna R, Micheli F, Woodson CB, Carr M, Malone D, Torre J, Boch C, Caselle JE, Edwards M, Freiwald J, *et al.* 2020. Geographic variation in responses of kelp forest communities of the California Current to recent climatic changes. *Global Change Biology* **26**: 6457–6473.

Beca-Carretero P, Azcárate-García T, Julia-Miralles M, Stanschewski CS, Guihéneuf F, Stengel DB. **2021**. Seasonal Acclimation Modulates the Impacts of Simulated Warming and Light Reduction on Temperate Seagrass Productivity and Biochemical Composition. *Frontiers in Marine Science* **8**.

Beca-Carretero P, Olesen B, Marbà N, Krause-Jensen D. **2018**. Response to experimental warming in northern eelgrass populations: comparison across a range of temperature adaptations. *Marine Ecology Progress Series* **589**: 59–72.

Beer S, Björk M, Beardall J. **2014**. *Photosynthesis in the marine environment*. John Wiley & Sons.

Bennett S, Alcoverro T, Kletou D, Antoniou C, Boada J, Buñuel X, Cucala L, Jorda G, Kleitou P, Roca G, *et al.* 2022. Resilience of seagrass populations to thermal stress does not reflect regional differences in ocean climate. *New Phytologist* **233**: 1657–1666.

Bennett S, Duarte CM, Marbà N, Wernberg T. **2019**. Integrating within-species variation in thermal physiology into climate change ecology. *Philosophical Transactions of the Royal Society B: Biological Sciences* **374**: 20180550.

Bond NA, Cronin MF, Freeland H, Mantua N. **2015**. Causes and impacts of the 2014 warm anomaly in the NE Pacific. *Geophysical Research Letters* **42**: 3414–3420.

Bonet-Melià P, Sandoval-Gil JM, Samperio-Ramos G, Vivanco-Bercovich M, Canino-Herrera SR, Durazo R, Camacho-Ibar VF, Alexandre A. **2023**. Marine heatwaves can limit the role of surfgrasses as biofilters for wastewaters. *Marine Pollution Bulletin* **196**.

Cael BB, Burger FA, Henson SA, Britten GL, Frölicher TL. **2024**. Historical and future maximum sea surface temperatures. *Science Advances* **10**: eadj5569.

Carlson DF, Yarbro LA, Scolaro S, Poniatowski M, McGee-Absten V, Carlson PR. **2018**. Sea surface temperatures and seagrass mortality in Florida Bay: Spatial and temporal patterns discerned from MODIS and AVHRR data. *Remote Sensing of Environment* **208**: 171–188.

Collier CJ, Waycott M. **2014**. Temperature extremes reduce seagrass growth and induce mortality. *Marine Pollution Bulletin* **83**: 483–490.

Cooper LW, McRoy CP. **1988**. Anatomical adaptations to rocky substrates and surf exposure by the seagrass genus *Phyllospadix*. *Aquatic Botany* **32**: 365–381.

Correia MJ, Osório ML, Osório J, Barrote I, Martins M, David MM. **2006**. Influence of transient shade periods on the effects of drought on photosynthesis, carbohydrate accumulation and lipid peroxidation in sunflower leaves. *Environmental and Experimental Botany* **58**: 75–84.

Costa MM, Silva J, Barrote I, Santos R. **2021**. Heatwave Effects on the Photosynthesis and Antioxidant Activity of the Seagrass *Cymodocea nodosa* under Contrasting Light Regimes. *Oceans* **2**: 448–460.

Deguette A, Barrote I, Silva J. **2022**. Physiological and morphological effects of a marine heatwave on the seagrass *Cymodocea nodosa*. *Scientific Reports* **12**: 7950.

Dennison WC. **1990**. Chlorophyll content. In: Phillips RC, McRoy CP, eds. Seagrass Research Methods. Paris, France: UNESCO.

Drysdale FR, Barbour MG. **1975**. Response of the marine angiosperm *Phyllospadix torreyi* to certain environmental variables: A preliminary study. *Aquatic Botany* **1**: 97–106.

Dubois M, Gilles KA, Hamilton JK, Rebers PA, Smith F. **1956**. Colorimetric method for determination of sugars and related substances. *Analytical Chemistry* **28**: 350–356.

Dunic JC, Brown CJ, Connolly RM, Turschwell MP, Côté IM. **2021**. Long-term declines and recovery of meadow area across the world's seagrass bioregions. *Global Change Biology* **27**: 4096–4109.

Entrambasaguas L, Ruocco M, Verhoeven KJF, Procaccini G, Marín-Guirao L. **2021**. Gene body DNA methylation in seagrasses: inter- and intraspecific differences and interaction with transcriptome plasticity under heat stress. *Scientific Reports* **11**: 14343.

Espinosa-Carreón TL, Gaxiola-Castro G, Robles-Pacheco JM, Nájera-Martínez S. **2001**. Temperature, salinity, nutrients and chlorophyll a in coastal waters of the Southern California Bight. *Ciencias Marinas* **27**: 397–422.

Fields JB, Silbiger NJ. **2022**. Foundation species loss alters multiple ecosystem functions within temperate tidepool communities. *Marine Ecology Progress Series* **683**: 1–19.

Foster NR, Apostolaki ET, DiBenedetto K, Duarte CM, Gregory D, Inostroza K, Krause-Jensen D, Jones BLH, Serrano E, Zakhama-Sraieb R, *et al.* 2025. Societal value of seagrass from historical to contemporary perspectives. *Ambio* **54**: 1289–1305.

Frölicher TL, Fischer EM, Gruber N. **2018**. Marine heatwaves under global warming. *Nature* **560**: 360–364.

García-Pantoja JA, Ruiz-Montoya L, Sandoval-Gil JM, Vivanco-Bercovich MV, Ferreira-Arrieta A, Zertuche-González JA, Guzmán-Calderón JM, Norzagaray-López Orión; Samperio-Ramos G, Montaño-Moctezuma G, Hernández-Ayón M. **2020**.

Fijación neta de carbono por pastos marinos (*Phyllospadix spp.*) en una isla del Pacífico Mexicano. In: Síntesis Nacionales. Estado Actual del Conocimiento del Ciclo del Carbono y sus Interacciones en México: Síntesis a 2020. Texcoco, Estado de México, México: Programa Mexicano del Carbono en colaboración con la Universidad Autónoma Metropolitana-Xochimilco, 602.

Gillis LG, Román S, Gustafsson C, Kauppi L, de los Santos CB, Varela Z, Viana IG. **2025**. The role of lag phases between real-term marine heatwaves in the trait responses of two macrophyte species. *Marine Environmental Research* **204**: 106894.

Gordillo FJL. **2012**. Environment and Algal Nutrition. In: Wiencke C, Bischof K, eds. Ecological Studies. Seaweed Biology. Berlin, Heidelberg: Springer Berlin Heidelberg, 67–86.

Gouvêa L, Fragkopoulou E, B. Araújo M, Serrão EA, Assis J. **2024**. Seagrass Biodiversity Under the Latest-Generation Scenarios of Projected Climate Change. *Journal of Biogeography* **52**: 172–185.

Gouvêa LP, Krause-Jensen D, Duarte CM, Assis J. **2025**. Projected impacts of future climate change on the aboveground biomass of seagrasses at global scale. *Science of The Total Environment* **966**: 178680.

Guerrero-Meseguer L, Marín A, Sanz-Lázaro C. **2017**. Future heat waves due to climate change threaten the survival of *Posidonia oceanica* seedlings. *Environmental Pollution* **230**: 40–45.

Gururani MA, Venkatesh J, Tran LSP. **2015**. Regulation of Photosynthesis during Abiotic Stress-Induced Photoinhibition. *Molecular Plant* **8**: 1304–1320.

Hartog C den, Kuo J. **2006**. Taxonomy and Biogeography of Seagrasses. In: Seagrasses: Biology, Ecology and Conservation. Dordrecht: Springer Netherlands, 1–23.

Hernán G, Ortega MJ, Gándara AM, Castejón I, Terrados J, Tomas F. **2017**. Future warmer seas: increased stress and susceptibility to grazing in seedlings of a marine habitat-forming species. *Global Change Biology* **23**: 4530–4543.

Hobday AJ, Alexander LV, Perkins SE, Smale DA, Straub SC, Oliver ECJ, Benthuysen JA, Burrows MT, Donat MG, Feng M, *et al.* 2016. A hierarchical approach to defining marine heatwaves. *Progress in Oceanography* **141**: 227–238.

Hobday AJ, Oliver EC, Gupta AS, Benthuysen JA, Burrows MT, Donat MG, Holbrook NJ, Moore PJ, Thomsen MS, Wernberg T. **2018**. Categorizing and naming marine heatwaves. *Oceanography* **31**: 162–173.

Hodges DM, DeLong JM, Forney CF, Prange RK. **1999**. Improving the thiobarbituric acid-reactive-substances assay for estimating lipid peroxidation in plant tissues containing anthocyanin and other interfering compounds. *Planta* **207**: 604–611.

IPCC. **2021**. *Climate Change 2021 – The Physical Science Basis: Working Group I Contribution to the Sixth Assessment Report of the Intergovernmental Panel on Climate Change*. Cambridge: Cambridge University Press.

Lawrence CM, Bolton JJ. **2022**. Experimental effects of warming and epiphyte grazing on the ecophysiology of two seagrass morphotypes. *Journal of Experimental Marine Biology and Ecology*: 151834.

Lichtenthaler HK, Wellburn AR. **1983**. Determinations of total carotenoids and chlorophylls a and b of leaf extracts in different solvents. *Biochemical Society Transactions* **11**: 591–592.

Litsi-Mizan V, Efthymiadis PT, Gerakaris V, Serrano O, Tsapakis M, Apostolaki ET. **2023**. Decline of seagrass *(Posidonia oceanica)* production over two decades in the face of warming of the Eastern Mediterranean Sea. *New Phytologist* **239**: 2126–2137.

Marbà N, Duarte CM. **2010**. Mediterranean warming triggers seagrass (*Posidonia oceanica*) shoot mortality. *Global Change Biology* **16**: 2366–2375.

Marbà N, Jordà G, Bennett S, Duarte CM. **2022**. Seagrass Thermal Limits and Vulnerability to Future Warming. *Frontiers in Marine Science* **9**.

Marín-Guirao L, Bernardeau-Esteller J, García-Muñoz R, Ramos A, Ontoria Y, Romero J, Pérez M, Ruiz JM, Procaccini G. **2018**. Carbon economy of Mediterranean seagrasses in response to thermal stress. *Marine Pollution Bulletin* **135**: 617–629.

Marín-Guirao L, Ruiz JM, Dattolo E, Garcia-Munoz R, Procaccini G. **2016**. Physiological and molecular evidence of differential short-term heat tolerance in Mediterranean seagrasses. *Scientific Reports* **6**: 28615.

Mathur S, Agrawal D, Jajoo A. **2014**. Photosynthesis: Response to high temperature stress. *Journal of Photochemistry and Photobiology B: Biology* **137**: 116–126.

Menge BA, Close SL, Hacker SD, Nielsen KJ, Chan F. **2020**. Biogeography of macrophyte productivity: Effects of oceanic and climatic regimes across spatiotemporal scales. *Limnology and Oceanography*: lno.11635.

Moore KA, Shields EC, Parrish DB. **2014**. Impacts of Varying Estuarine Temperature and Light Conditions on *Zostera marina* (Eelgrass) and its Interactions With *Ruppia maritima* (Widgeongrass). *Estuaries and Coasts* **37**: 20–30.

Murchie EH, Ruban AV. **2020**. Dynamic non-photochemical quenching in plants: from molecular mechanism to productivity. *The Plant Journal* **101**: 885–896.

Mvungi EF, Pillay D. **2019**. Eutrophication overrides warming as a stressor for a temperate African seagrass (*Zostera capensis*). *PLOS ONE* **14**: e0215129.

Nguyen HM, Kim M, Ralph PJ, Marín-Guirao L, Pernice M, Procaccini G. **2020**. Stress Memory in Seagrasses: First Insight Into the Effects of Thermal Priming and the Role of Epigenetic Modifications. *Frontiers in Plant Science* **11**: 494.

Nguyen HM, Ralph PJ, Marín-Guirao L, Pernice M, Procaccini G. **2021**. Seagrasses in an era of ocean warming: a review. *Biological Reviews* **96**: 2009–2030.

Oliver ECJ, Burrows MT, Donat MG, Sen Gupta A, Alexander LV, Perkins-Kirkpatrick SE, Benthuysen JA, Hobday AJ, Holbrook NJ, Moore PJ, *et al.* 2019. Projected Marine Heatwaves in the 21st Century and the Potential for Ecological Impact. *Frontiers in Marine Science* **6**.

Olsen YS, Sánchez-Camacho M, Marbà N, Duarte CM. **2012**. Mediterranean Seagrass Growth and Demography Responses to Experimental Warming. *Estuaries and Coasts* **35**: 1205–1213.

Pazzaglia J, Badalamenti F, Bernardeau-Esteller J, Ruiz JM, Giacalone VM, Procaccini G, Marín-Guirao L. 2022. Thermo-priming increases heat-stress tolerance in seedlings of the Mediterranean seagrass *P. oceanica*. *Marine Pollution Bulletin* **174**: 113164.

Pazzaglia J, Reusch TBH, Terlizzi A, Marín-Guirao L, Procaccini G. 2021. Phenotypic plasticity under rapid global changes: The intrinsic force for future seagrasses survival. *Evolutionary Applications* **14**: 1181–1201.

R Core Team. 2020. R: A language and environment for statistical computing. *R Foundation for Statistical Computing*.

Ramírez-García P, Lot A, Duarte C, Terrados J, Agawin N. 1998. Bathymetric distribution, biomass and growth dynamics of intertidal *Phyllospadix scouleri* and *Phyllospadix torreyi* in Baja California (Mexico). *Marine Ecology Progress Series* **173**: 13–23.

Rinaldi A, Martinez M, Badalamenti F, D'Anna G, Mirto S, Marín-Guirao L, Procaccini G, Montalto V. 2023. The ontogeny-specific thermal sensitivity of the seagrass *Posidonia oceanica*. *Frontiers in Marine Science* **10**.

Ruiz-Montoya L, Sandoval-Gil JM, Belando-Torrentes MD, Vivanco-Bercovich M, Cabello-Pasini A, Rangel-Mendoza LK, Maldonado-Gutiérrez A, Ferrerira-Arrieta A, Guzmán-Calderón JM. 2021. Ecophysiological responses and self-protective canopy effects of surfgrass (*Phyllospadix torreyi*) in the intertidal. *Marine Environmental Research* **172**: 105501.

Ruocco M, De Luca P, Marín-Guirao L, Procaccini G. 2019. Differential Leaf Age-Dependent Thermal Plasticity in the Keystone Seagrass *Posidonia oceanica*. *Frontiers in Plant Science* **10**: 1556.

Ruocco M, Entrambasaguas L, Dattolo E, Milito A, Marín-Guirao L, Procaccini G. 2021. A king and vassals' tale: Molecular signatures of clonal integration in *Posidonia oceanica* under chronic light shortage (C Angelini, Ed.). *Journal of Ecology* **109**: 294–312.

Sabeena Farvin KH, Jacobsen C. 2013. Phenolic compounds and antioxidant activities of selected species of seaweeds from Danish coast. *Food Chemistry* **138**: 1670–1681.

Saha M, Barboza FR, Somerfield PJ, Al-Janabi B, Beck M, Brakel J, Ito M, Pansch C, Nascimento-Schulze JC, Jakobsson Thor S, *et al.* 2020. Response of foundation macrophytes to near-natural simulated marine heatwaves. *Global Change Biology* **26**: 417–430.

Sandoval-Gil J, Alexandre A, Santos R, Camacho-Ibar VF. **2016**. Nitrogen Uptake and Internal Recycling in *Zostera marina* Exposed to Oyster Farming: Eelgrass Potential as a Natural Biofilter. *Estuaries and Coasts* **39**: 1694–1708.

Singleton VL, Rossi JA. **1965**. Colorimetry of Total Phenolics with Phosphomolybdic-Phosphotungstic Acid Reagents. *American Journal of Enology and Viticulture* **16**: 144–158.

Starko S, Van Der Mheen M, Pessarrodona A, Wood GV, Filbee-Dexter K, Neufeld CJ, Montie S, Coleman MA, Wernberg T. **2024**. Impacts of marine heatwaves in coastal ecosystems depend on local environmental conditions. *Global Change Biology* **30**: e17469.

Stipcich P, Marín-Guirao L, Pansini A, Pinna F, Procaccini G, Pusceddu A, Soru S, Ceccherelli G. **2022a**. Effects of Current and Future Summer Marine Heat Waves on *Posidonia oceanica*: Plant Origin Matters? *Frontiers in Climate* **4**: 844831.

Stipcich P, Pansini A, Beca-Carretero P, Stengel DB, Ceccherelli G. **2022b**. Field thermo acclimation increases the resilience of *Posidonia oceanica* seedlings to marine heat waves. *Marine Pollution Bulletin* **184**: 114230.

Strydom S, Mccallum R, Lafratta A, Webster C, O'Dea C, Said N, Dunham N, Inostroza K, Salinas C, Billinghurst S, *et al.* 2023. Global dataset on seagrass meadow structure, biomass and production. *Earth System Science Data* **15**: 511–519.

Strydom S, Murray K, Wilson S, Huntley B, Rule M, Heithaus M, Bessey C, Kendrick GA, Burkholder D, Fraser MW, *et al.* 2020. Too hot to handle: Unprecedented seagrass death driven by marine heatwave in a World Heritage Area. *Global Change Biology* **26**: 3525–3538.

Tavares AI, Assis J, Anderson L, Raimondi P, Coelho NC, Paulino C, Ladah L, Nakaoka M, Pearson GA, Serrao EA. **2024**. Past and future climate effects on population structure and diversity of North Pacific surfgrasses. *Journal of Biogeography* **51**: 1999–2010.

Tharaldson T. **2018**. The ability of *Phyllospadix spp.*, a pair of intertidal foundation species, to maintain biodiversity and ameliorate CO_2 stress in rocky shore tidepools. *Cal Poly Humboldt theses and projects*.

Thomson JA, Burkholder DA, Heithaus MR, Fourqurean JW, Fraser MW, Statton J, Kendrick GA. **2015**. Extreme temperatures, foundation species, and abrupt ecosystem change: an example from an iconic seagrass ecosystem. *Global Change Biology* **21**: 1463–1474.

Touchette BW, Burkholder JM. **2007**. Carbon and nitrogen metabolism in the seagrass, *Zostera marina* L.: Environmental control of enzymes involved in carbon allocation and nitrogen assimilation. *Journal of Experimental Marine Biology and Ecology* **350**: 216–233.

Unsworth RK, Cullen-Unsworth LC, Jones BL, Lilley RJ. **2022**. The planetary role of seagrass conservation. *Science* **377**: 609–613.

Vivanco-Bercovich M, Belando-Torrentes MD, Figueroa-Burgos MF, Ferreira-Arrieta A, Macías-Carranza V, García-Pantoja JA, Cabello-Pasini A, Samperio-Ramos G, Cruz-López R, Sandoval-Gil JM. **2022**. Combined effects of marine heatwaves and reduced light on the physiology and growth of the surfgrass *Phyllospadix torreyi* from Baja California, Mexico. *Aquatic Botany* **178**: 103488.

Vivanco-Bercovich M, Sandoval-Gil JM, Bonet-Meliá P, Cabello-Pasini A, Muñiz-Salazar R, Montoya LR, Schubert N, Marín-Guirao L, Procaccini G, Ferreira-Arrieta A. **2024**. Marine heatwaves recurrence aggravates thermal stress in the surfgrass *Phyllospadix scouleri*. *Marine Pollution Bulletin* **199**: 115943.

Wei X, Li K, Kilpatrick T, Wang M, Xie S. **2021**. Large-Scale Conditions for the Record-Setting Southern California Marine Heatwave of August 2018. *Geophysical Research Letters* **48**.

Zieman JC. **1974**. Methods for the study of the growth and production of turtle grass, *Thalassia testudinum* König. *Aquaculture* **4**: 139–143.

736

Tables

Table 1. Results of two-way ANOVA testing the effects of treatment (Trt., 3 levels: Control, HW-1, HW-2), experimental phase (E.P., 2 levels: T-1 and T-2), and their interaction (Int.) on all biological descriptors. Significance codes: *p < 0.05; **p < 0.01; ***p < 0.001, n.s. p > 0.05.

Variable	Effect	F - value	p - value	Variable	Effect	F - value	p - value
Net-P_{max}	Trt.	9.464	**	**Nitrate uptake rate**	Trt.	35.508	***
	E. P.	37.07	***		E. P.	88.727	***
	Int.	1.04	n.s.		Int.	81.401	***
Gross-P_{max}	Trt.	3.007	n.s.	**NRA**	Trt.	118.176	***
	E. P.	34.927	***		E. P.	47.203	***
	Int.	0.947	n.s.		Int.	527.508	***
E_k	Trt.	8.573	**	**Chl. *a***	Trt.	1.599	n.s.
	E. P.	38.006	***		E. P.	0.526	n.s.
	Int.	0.464	n.s.		Int.	1.628	n.s.
α	Trt.	0.635	n.s.	**Chl. *b***	Trt.	1.751	n.s.
	E. P.	0.029	n.s.		E. P.	0.269	n.s.
	Int.	2.661	n.s.		Int.	1.848	n.s.
E_c	Trt.	10.971	***	**Chl. *b/a* ratio**	Trt.	2.572	n.s.
	E. P.	1.24	n.s.		E. P.	0.003	n.s.
	Int.	1.182	n.s.		Int.	0.028	n.s.
R	Trt.	9.78	**	**Carotenoids**	Trt.	0.014	n.s.
	E. P.	2.005	n.s.		E. P.	17.55	***
	Int.	0.368	n.s.		Int.	3.283	n.s.
F_v/F_m	Trt.	7.898	**	**Phenolic content**	Trt.	6.149	**
	E. P.	14.279	**		E. P.	6.696	*
	Int.	1.272	n.s.		Int.	2.019	n.s.
$Φ_{PSII}$	Trt.	13.306	***	**Antioxidant capacity**	Trt.	6.898	**
	E. P.	25.243	***		E. P.	12.276	**
	Int.	12.045	***		Int.	2.283	n.s.
ETR	Trt.	28.368	***	**Lipid peroxidation**	Trt.	5.111	*
	E. P.	148.013	***		E. P.	0.292	n.s.
	Int.	6.212	**		Int.	3.875	*
F_0	Trt.	2.723	**	**NSCs**	Trt.	2.338	n.s.
	E. P.	0.586	n.s.		E. P.	0.005	n.s.
	Int.	0.653	n.s.		Int.	3.005	n.s.
F_m	Trt.	70.167	***	**DP**	Trt.	14.39	***
	E. P.	24.62	***		E. P.	0.009	n.s.
	Int.	7.109	**		Int.	0.557	n.s.
NPQ	Trt.	4.224	*	**RGR**	Trt.	30.962	***
	E. P.	1.453	n.s.		E. P.	1.979	n.s.
	Int.	0.083	n.s.		Int.	0.726	n.s.

743 **Table 2.** Mean (± SE) values of pigment concentration (chlorophyll *a*, chlorophyll *b*, Chl *b/a*
744 ratio, carotenoids), phenolic content, antioxidant capacity, and lipid peroxidation across
745 treatments (Control, Severe, Extreme) and experimental phases (Warming and Post-
746 warming). Letters in parentheses indicate statistically significant differences based on post
747 hoc comparisons ($p < 0.05$). Uppercase letters denote differences among treatments;
748 lowercase letters indicate interaction effects.

Variable	**Treatment**	**Experimental phase**	
		Warming	Post-warming
Chlorophyll *a*	Control	1.1 ± 0.07	1.02 ± 0.04
	Severe	1.37 ± 0.13	1.12 ± 0.18
	Extreme	1.11 ± 0.1	1.24 ± 0.03
Chlorophyll *b*	Control	0.49 ± 0.03	0.47 ± 0.01
	Severe	0.55 ± 0.03	0.47 ± 0.08
	Extreme	0.52 ± 0.04	0.59 ± 0.02
Chl. *b/a* ratio	Control	0.44 ± 0.01	0.45 ± 0.01
	Severe	0.41 ± 0.01	0.41 ± 0.01
	Extreme	0.45 ± 0.03	0.44 ± 0.01
Carotenoids	Control	0.27 ± 0	0.27 ± 0.01
	Severe	0.31 ± 0.02	0.26 ± 0.03
	Extreme	0.28 ± 0.03	0.35 ± 0
Phenolic content	Control (A)	5.9 ± 0.35	6.12 ± 0.63
	Severe (B)	4.3 ± 0.13	5.82 ± 0.34
	Extreme (B)	4.66 ± 0.24	5.1 ± 0.1
Antioxidant capacity	Control (A)	2.77 ± 0.49	3.15 ± 0.29
	Severe (AB)	1.69 ± 0.06	3.11 ± 0.2
	Extreme (B)	1.72 ± 0.21	2.22 ± 0.14
Lipid peroxidation	Control	29.86 ± 1.24 (a)	29.58 ± 1.98 (a)
	Severe	20.75 ± 1.85 (b)	27.71 ± 1.72 (a)
	Extreme	31.86 ± 2.02 (a)	27.84 ± 2.86 (a)

749

Figure legends

Figure 1. (A) Location of the *Phyllospadix scouleri* donor meadow at Todos Santos Island, Baja California, Mexico, and (B) representative photo of the meadow. (C) Seawater temperatures recorded over two years using submersible loggers at 15-minute intervals. Solid lines show daily average (black), maximum (red), and minimum (blue) temperatures. Satellite SST data (dotted line) were retrieved from NOAA (High-Resolution SST data), and MHWs (black bars) were identified using the Marine Heatwave Tracker (Schlegel et al., 2020). (D) Experimental temperature profiles for Control, Severe-MHW, and Extreme-MHW treatments across the acclimation, warming, and post-warming phases. Sampling time points for biological descriptors are indicated with white dots. Background shading corresponds to MHW categories based on climatological thresholds (Hobday et al., 2018).

Figure 2. Photosynthesis–irradiance curve derived measured in *Phyllospadix scouleri* under three temperature treatments: Control (18.5 ± 1.5°C), Severe-MHW (23.5 ± 1.5°C) and Extreme-MHW (26.5 ± 1.5°C). Measurements were taken at the end of the warming and post-warming phases. Bars represent mean ± SE (n = 4). Two-way ANOVA results for treatment, experimental phase, and their interaction are shown. Significant differences among treatments ($p < 0.05$, Tukey HSD) are indicated by different uppercase letters when the main effect of treatment was significant. See Table 1 for full statistical results. Variables: (A) Net maximum photosynthetic rate (Net-P_{max}), (B) Gross-P_{max}, (C) Saturation irradiance (E_k), (D) Photosynthetic efficiency (α), (E) Compensation irradiance (E_c), (F) Respiration rate (R).

Figure 3. Photochemistry parameters measured in *Phyllospadix scouleri* under three temperature treatments: Control (18.5 ± 1.5°C), Severe-MHW (23.5 ± 1.5°C) and Extreme-MHW (26.5 ± 1.5°C). Measurements were taken at the end of the warming and post-warming phases. Bars represent mean ± SE (n = 4). Two-way ANOVA results for treatment, experimental phase, and their interaction are shown. Significant differences among treatments (Tukey HSD, $p < 0.05$) are indicated with uppercase letters when the main effect of treatment was significant, and with lowercase letters for pairwise comparisons among treatments within each phase when a significant interaction was detected. See Table 1 for full statistical results. Variables: (A) Maximum quantum yield (F_v/F_m), (B) Effective quantum

780 yield (Φ_{PSII}), (C) Electron transport rate (ETR), (D) Basal fluorescence (F_0), (E) Maximum
781 fluorescence (F_m), (F) Non-photochemical quenching (NPQ).

782 **Figure 4.** Nitrogen metabolism in *Phyllospadix scouleri* under three temperature treatments:
783 Control (18.5 ± 1.5 °C), Severe-MHW (23.5 ± 1.5 °C), and Extreme-MHW (26.5 ± 1.5 °C).
784 Measurements were taken at the end of the warming and post-warming phases. Bars represent
785 mean ± SE (n = 4). Two-way ANOVA results for treatment, experimental phase, and their
786 interaction are shown. When a significant interaction was detected, lowercase letters indicate
787 significant pairwise differences among treatments within each phase (Tukey HSD, $p < 0.05$).
788 See Table 1 for full statistical results. Variables: (A) Nitrate uptake rate at 5 μM, (B) Nitrate
789 reductase activity (NRA).

790 **Figure 5.** Energy and growth metrics measured in *P. scouleri* under three temperature
791 treatments: Control (18.5 ± 1.5°C), Severe-MHW (23.5 ± 1.5°C) and Extreme-MHW
792 (26.5 ± 1.5°C). Measurements were taken at the end of the warming and post-warming
793 phases. Bars represent mean ± SE (n = 4). Two-way ANOVA results for treatment,
794 experimental phase, and their interaction are shown. Significant differences among
795 treatments ($p < 0.05$, Tukey HSD) are indicated by different uppercase letters when the main
796 effect of treatment was significant. See Table 1 for full statistical results. Variables: (A) Non-
797 structural carbohydrates (NSC), (B) Daily productivity (DP), (C) Relative growth rate
798 (RGR).

799 **Figure 6.** Principal Component Analysis (PCA) performed with the physiological responses
800 of *Phyllospadix scouleri* to three temperature treatments: Control (18.5 ± 1.5°C), Severe-
801 MHW (23.5 ± 1.5°C) and Extreme-MHW (26.5 ± 1.5°C). Measurements were taken at the
802 end of the warming and post-warming phases. The first two principal components explain
803 56.2% of the total variance (PC1: 31.8%, PC2: 24.4%). Arrows represent loadings of key
804 physiological variables contributing to each axis. See Table S4 for further PCA details.

Figures

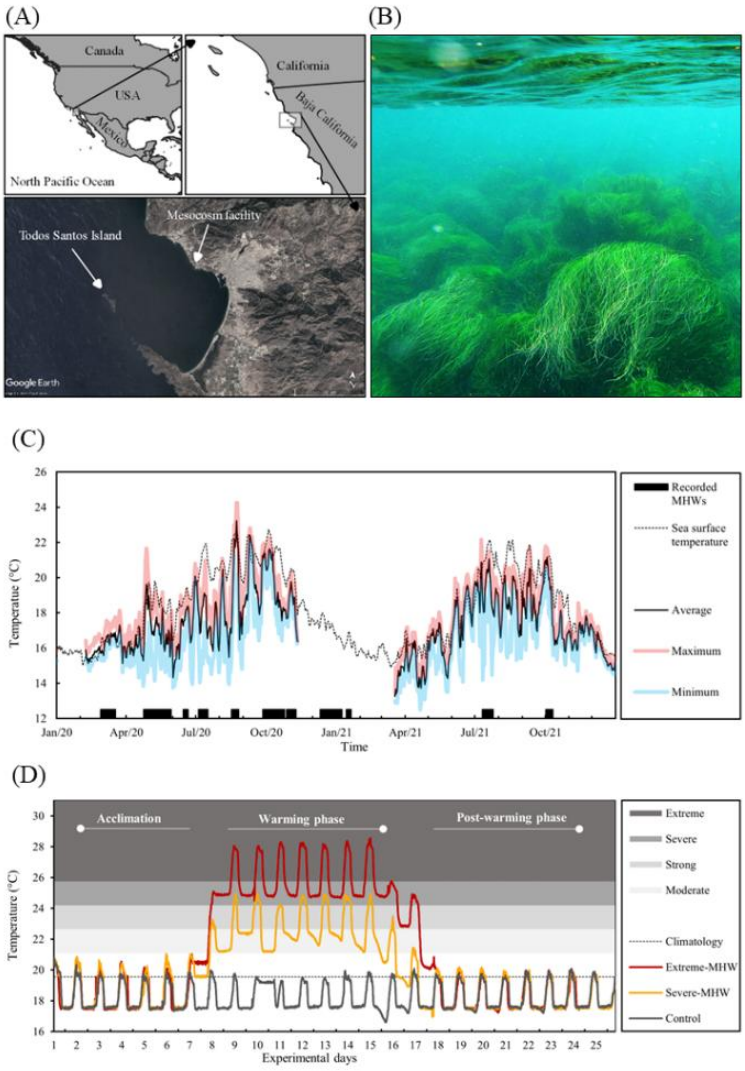

Figure 1. (A) Location of the *Phyllospadix scouleri* donor meadow at Todos Santos Island, Baja California, Mexico, and (B) representative photo of the meadow. (C) Seawater temperatures recorded over two years using submersible loggers at 15-minute intervals. Solid lines show daily average (black), maximum (red), and minimum (blue) temperatures. Satellite SST data (dotted line) were retrieved from NOAA (High-Resolution SST data), and MHWs (black bars) were identified using the Marine Heatwave Tracker (Schlegel et al., 2020). (D) Experimental temperature profiles for Control, Severe-MHW, and Extreme-MHW treatments across the acclimation, warming, and post-warming phases. Sampling time points for biological descriptors are indicated with white dots. Background shading corresponds to MHW categories based on climatological thresholds (Hobday et al., 2018).

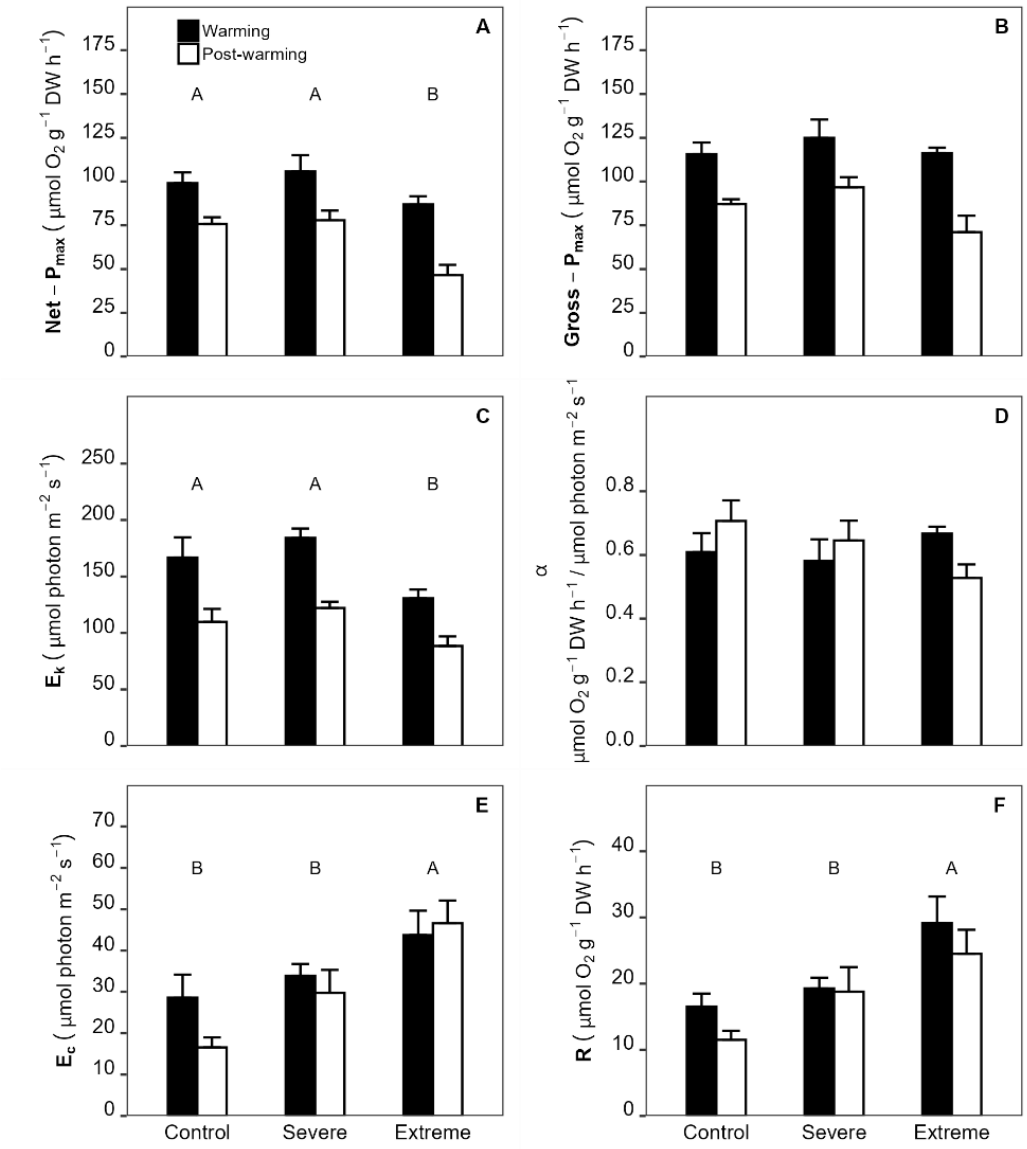

Figure 2. Photosynthesis–irradiance curve derived measured in *Phyllospadix scouleri* under three temperature treatments: Control (18.5 ± 1.5°C), Severe-MHW (23.5 ± 1.5°C) and Extreme-MHW (26.5 ± 1.5°C). Measurements were taken at the end of the warming and post-warming phases. Bars represent mean ± SE (n = 4). Two-way ANOVA results for treatment, experimental phase, and their interaction are shown. Significant differences among treatments ($p < 0.05$, Tukey HSD) are indicated by different uppercase letters when the main effect of treatment was significant. See Table 1 for full statistical results. Variables: (A) Net maximum photosynthetic rate (Net-P_{max}), (B) Gross-P_{max}, (C) Saturation irradiance (E_k), (D) Photosynthetic efficiency (α), (E) Compensation irradiance (E_c), (F) Respiration rate (R).

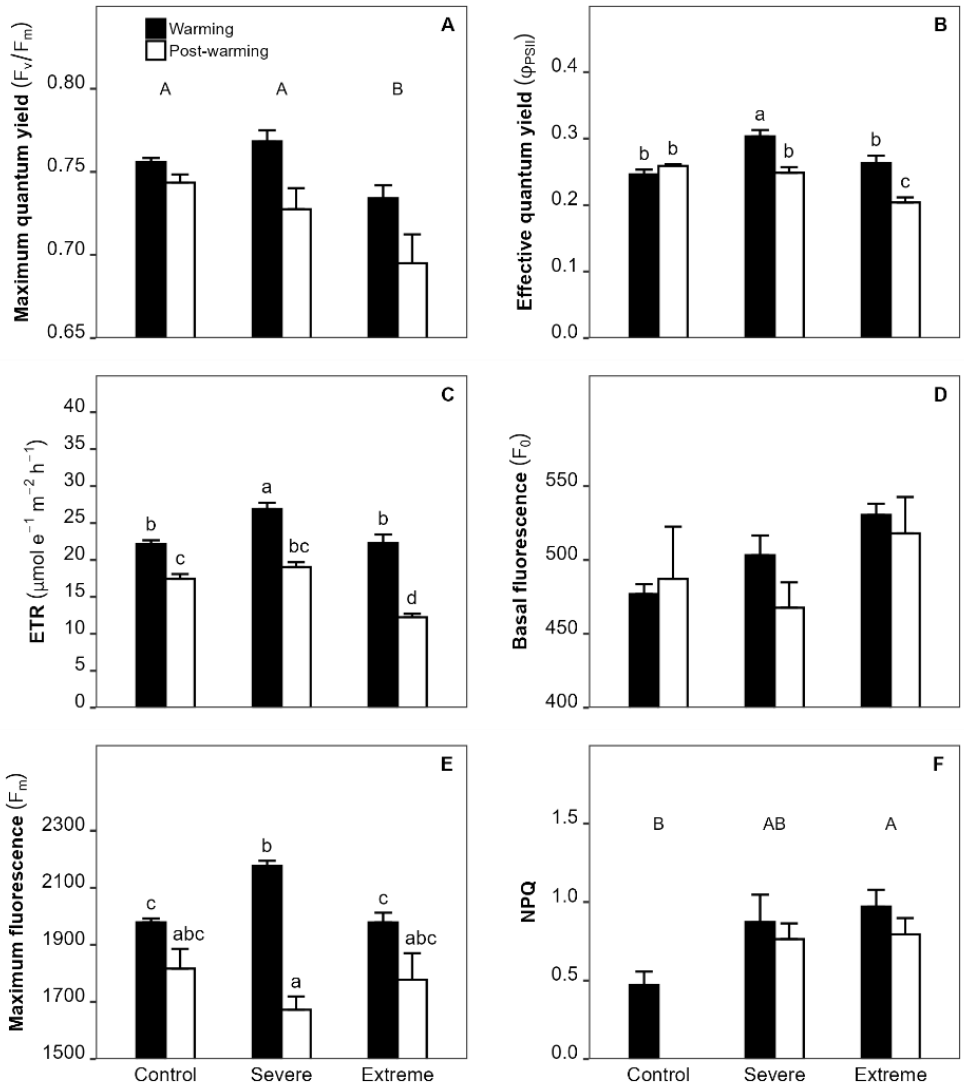

Figure 3. Photochemistry parameters measured in *Phyllospadix scouleri* under three temperature treatments: Control (18.5 ± 1.5°C), Severe-MHW (23.5 ± 1.5°C) and Extreme-MHW (26.5 ± 1.5°C). Measurements were taken at the end of the warming and post-warming phases. Bars represent mean ± SE (n = 4). Two-way ANOVA results for treatment, experimental phase, and their interaction are shown. Significant differences among treatments (Tukey HSD, $p < 0.05$) are indicated with uppercase letters when the main effect of treatment was significant, and with lowercase letters for pairwise comparisons among treatments within each phase when a significant interaction was detected. See Table 1 for full statistical results. Variables: (A) Maximum quantum yield (F_v/F_m), (B) Effective quantum yield (Φ_{PSII}), (C) Electron transport rate (ETR), (D) Basal fluorescence (F_0), (E) Maximum fluorescence (F_m), (F) Non-photochemical quenching (NPQ).

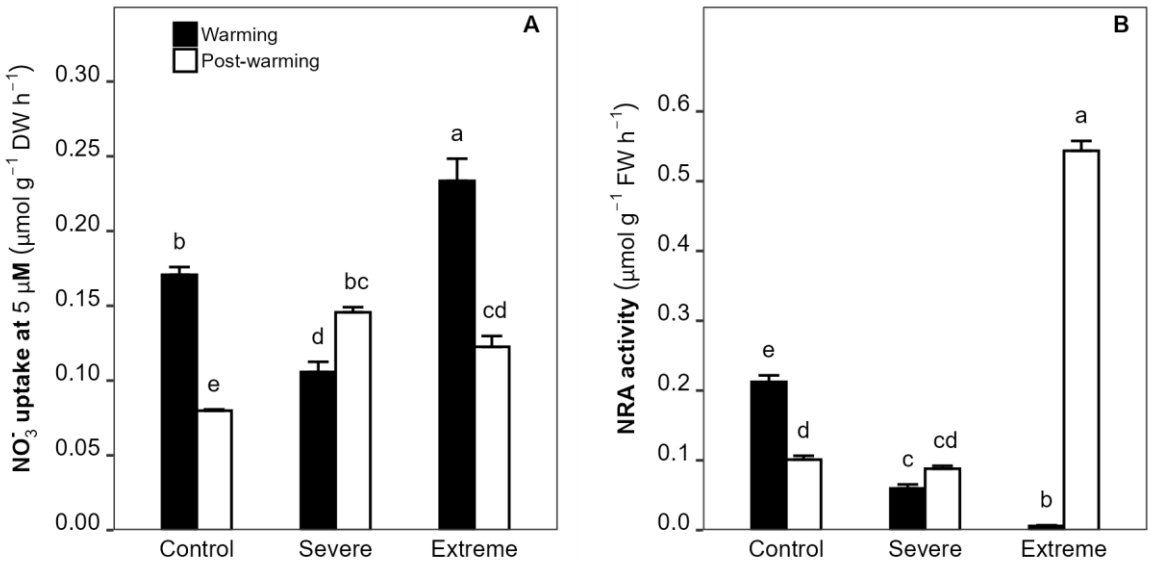

841

842 **Figure 4.** Nitrogen metabolism in *Phyllospadix scouleri* under three temperature treatments:
843 Control (18.5 ± 1.5 °C), Severe-MHW (23.5 ± 1.5 °C), and Extreme-MHW (26.5 ± 1.5 °C).
844 Measurements were taken at the end of the warming and post-warming phases. Bars represent
845 mean ± SE (n = 4). Two-way ANOVA results for treatment, experimental phase, and their
846 interaction are shown. When a significant interaction was detected, lowercase letters indicate
847 significant pairwise differences among treatments within each phase (Tukey HSD, $p < 0.05$).
848 See Table 1 for full statistical results. Variables: (A) Nitrate uptake rate at 5 µM, (B) Nitrate
849 reductase activity (NRA).

850

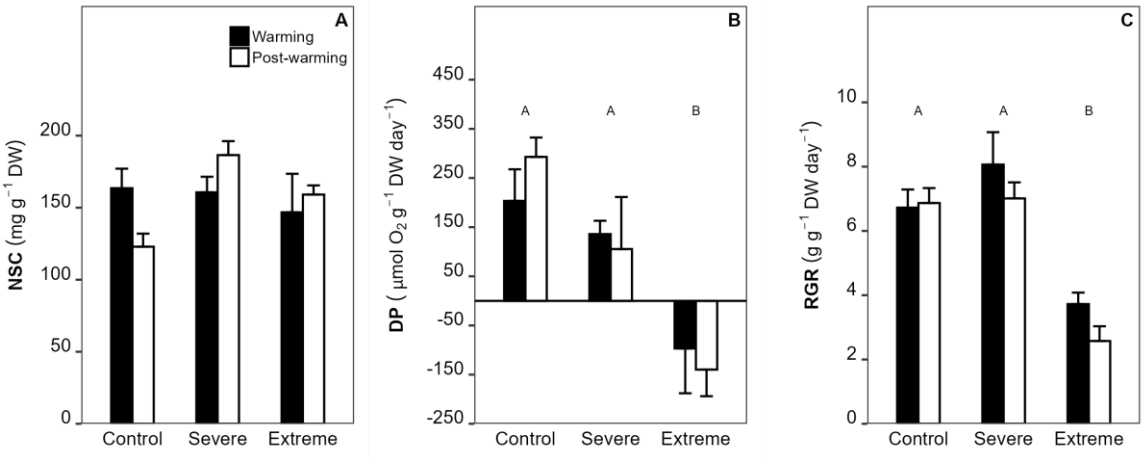

Figure 5. Energy and growth metrics measured in *P. scouleri* under three temperature treatments: Control (18.5 ± 1.5°C), Severe-MHW (23.5 ± 1.5°C) and Extreme-MHW (26.5 ± 1.5°C). Measurements were taken at the end of the warming and post-warming phases. Bars represent mean ± SE (n = 4). Two-way ANOVA results for treatment, experimental phase, and their interaction are shown. Significant differences among treatments ($p < 0.05$, Tukey HSD) are indicated by different uppercase letters when the main effect of treatment was significant. See Table 1 for full statistical results. Variables: (A) Non-structural carbohydrates (NSC), (B) Daily productivity (DP), (C) Relative growth rate (RGR).

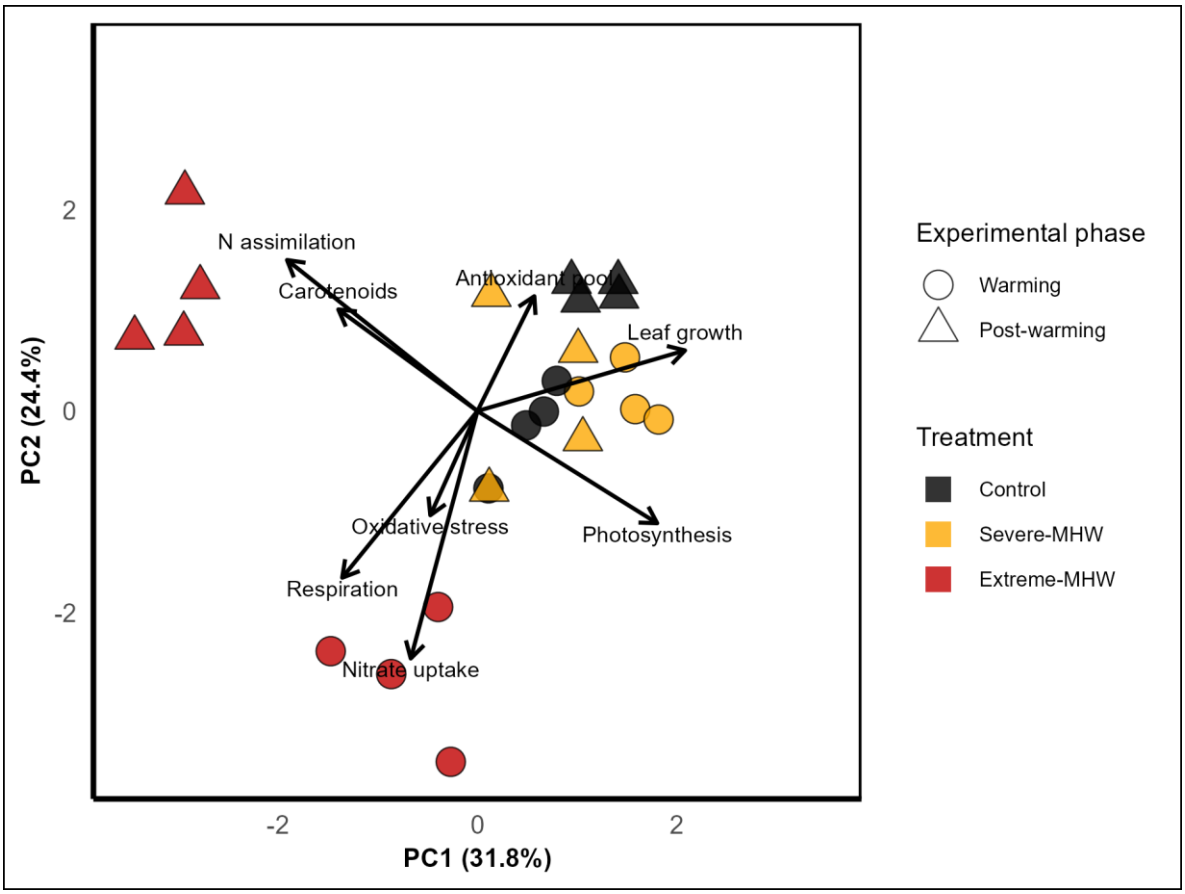

862

863 **Figure 6.** Principal Component Analysis (PCA) performed with the physiological
864 responses of *Phyllospadix scouleri* to three temperature treatments: Control (18.5 ± 1.5°C),
865 Severe-MHW (23.5 ± 1.5°C) and Extreme-MHW (26.5 ± 1.5°C). Measurements were taken
866 at the end of the warming and post-warming phases. The first two principal components
867 explain 56.2% of the total variance (PC1: 31.8%, PC2: 24.4%). Arrows represent loadings
868 of key physiological variables contributing to each axis. See Table S4 for further PCA
869 details.

(A)

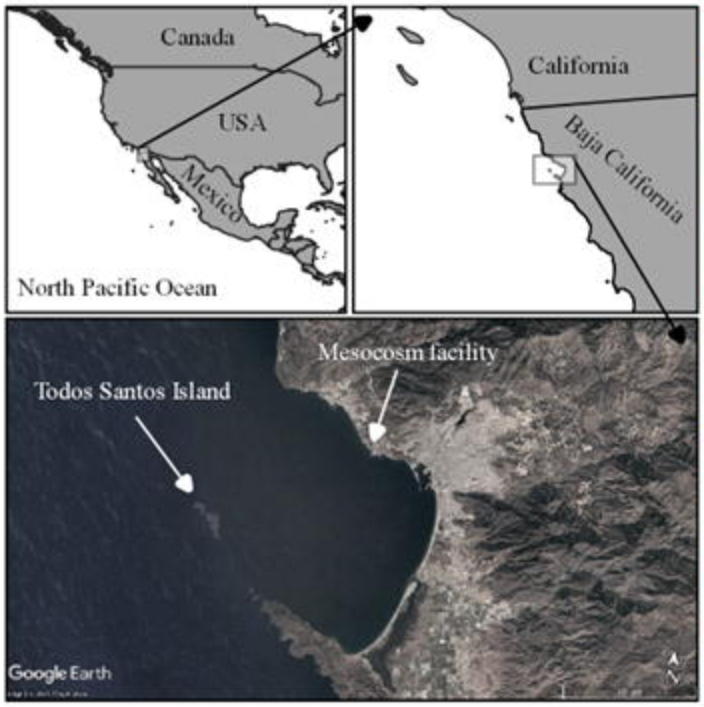

(B)

(C)

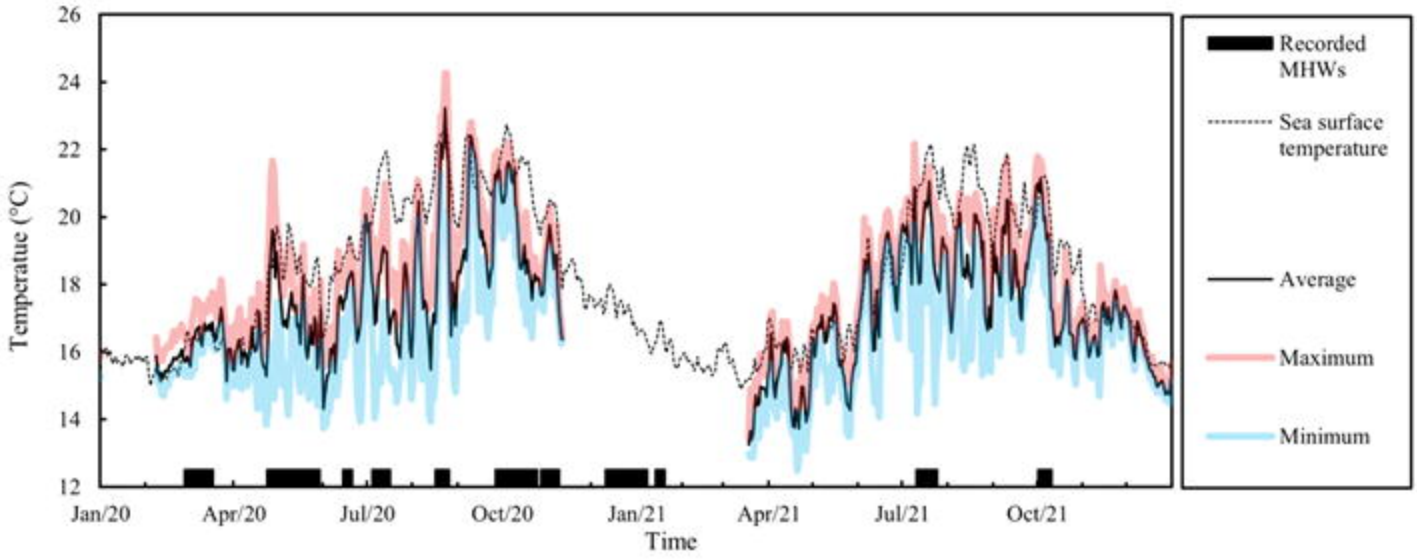

(D)

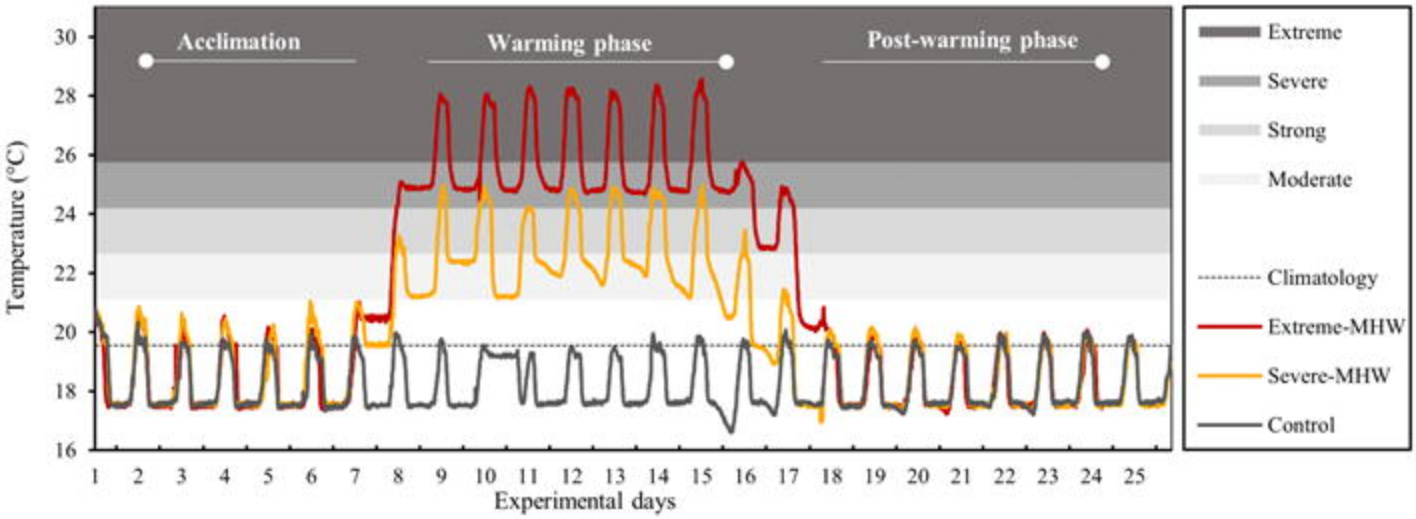

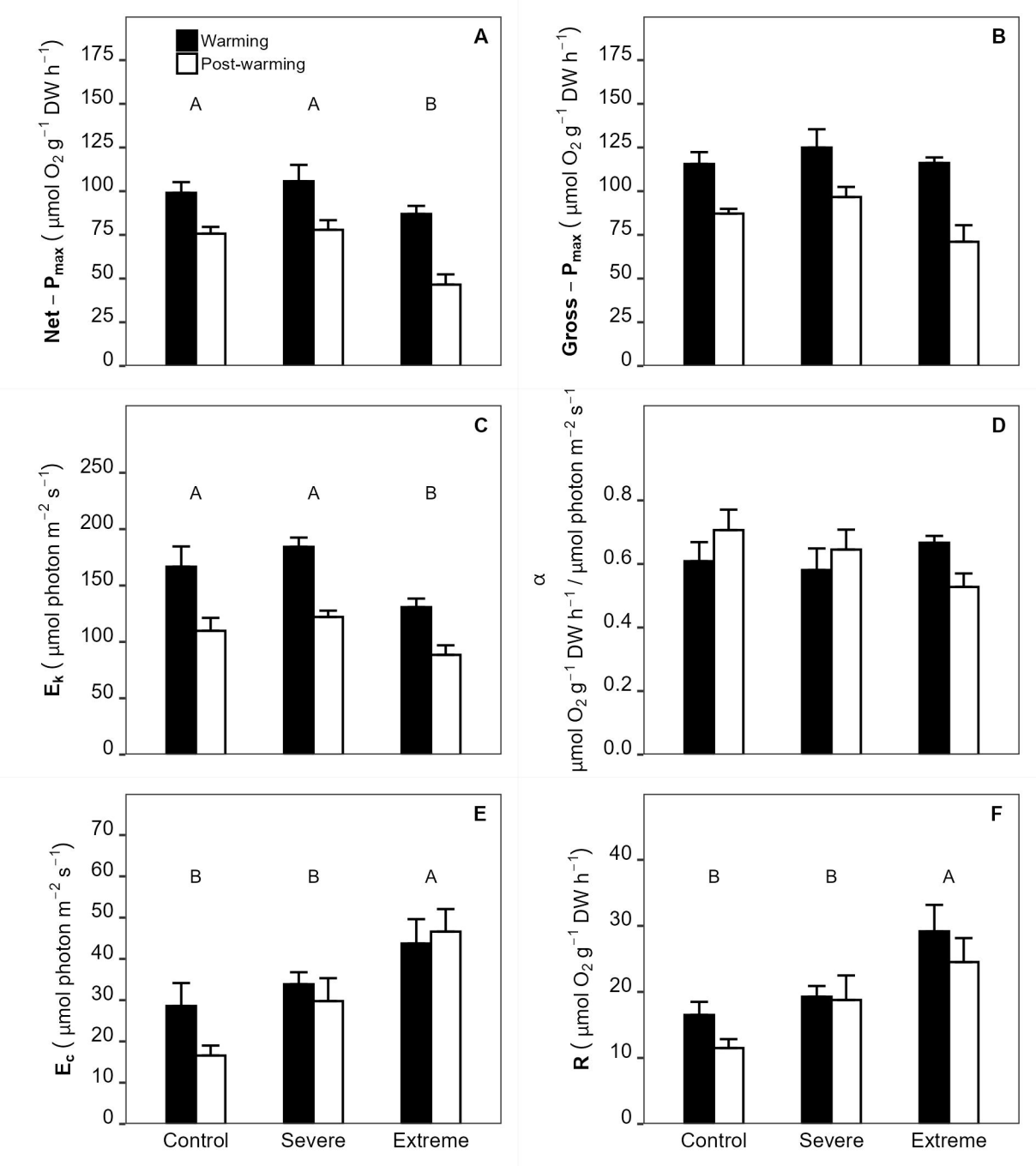
A
Warming
Post-warming
Net – P_{max} (µmol O_2 g^{-1} DW h^{-1})
175
150
125
100
75
50
25
0
A
A
B
B
Gross – P_{max} (µmol O_2 g^{-1} DW h^{-1})
C
E_k (µmol photon m^{-2} s^{-1})
250
200
150
100
50
D
α
µmol O_2 g^{-1} DW h^{-1} / µmol photon m^{-2} s^{-1}
0.8
0.6
0.4
0.2
0.0
E
E_c (µmol photon m^{-2} s^{-1})
70
60
50
40
30
20
10
F
R (µmol O_2 g^{-1} DW h^{-1})
Control
Severe
Extreme

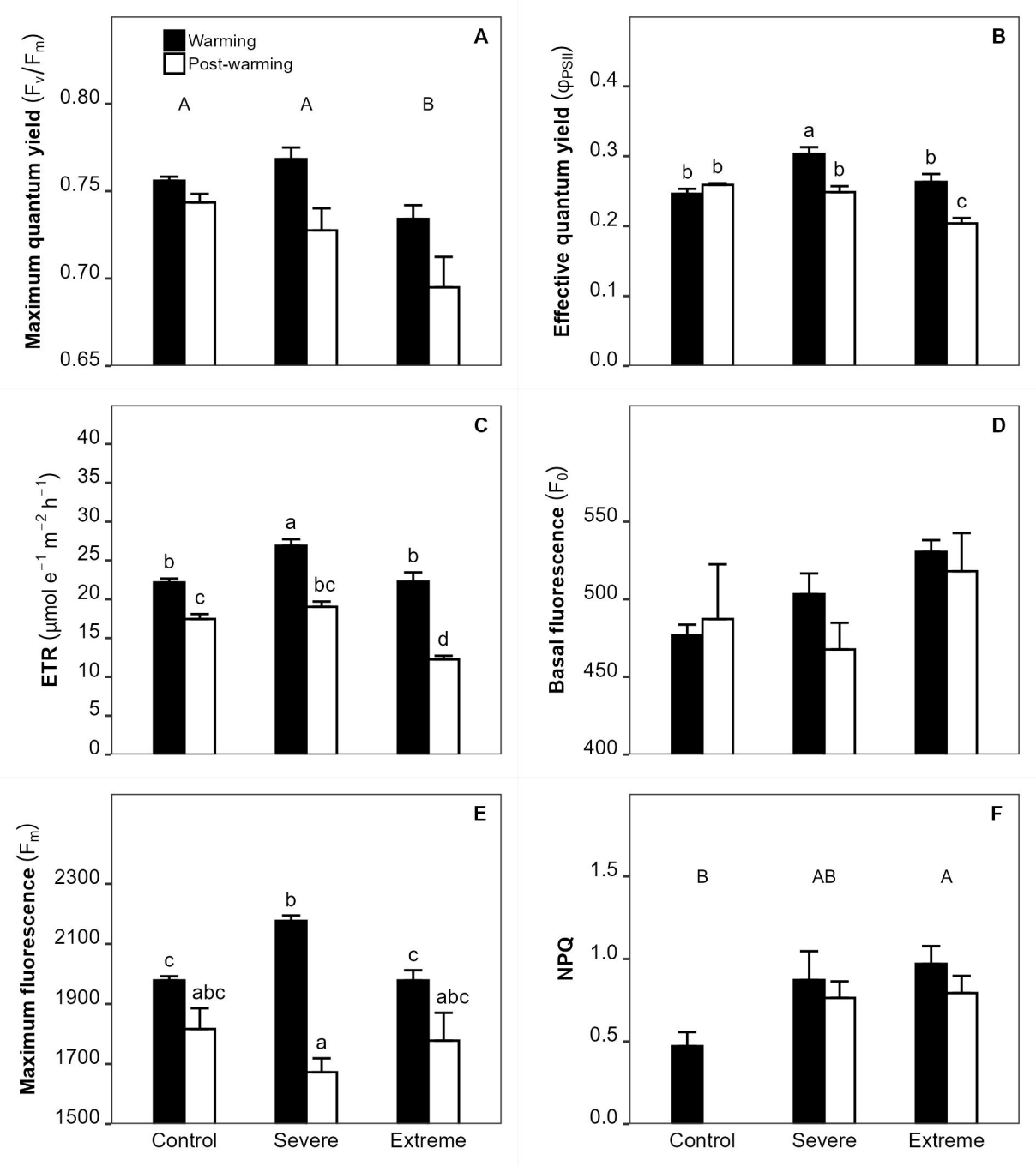
A
Warming
Post-warming
Maximum quantum yield (F_v/F_m)
0.80
0.75
0.70
0.65
A
A
B
B
Effective quantum yield (φ_{PSII})
0.4
0.3
0.2
0.1
0.0
b
b
a
b
b
c
C
ETR (μmol e^{-1} m^{-2} h^{-1})
40
35
30
25
20
15
10
5
0
b
c
a
bc
b
d
D
Basal fluorescence (F_0)
550
500
450
400
E
Maximum fluorescence (F_m)
2300
2100
1900
1700
1500
c
abc
b
a
c
abc
Control
Severe
Extreme
F
NPQ
1.5
1.0
0.5
0.0
B
AB
A
Control
Severe
Extreme

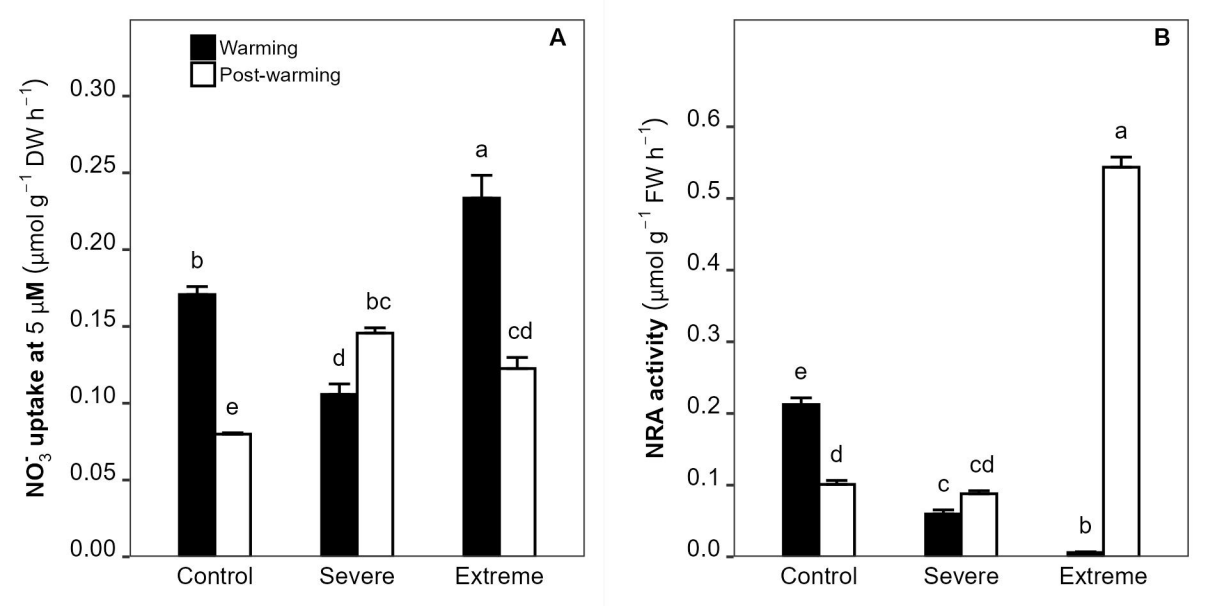
A
Warming
Post-warming
NO_3^- uptake at 5 μM (μmol g^{-1} DW h^{-1})
0.00
0.05
0.10
0.15
0.20
0.25
0.30
b
e
d
bc
a
cd
Control
Severe
Extreme
B
NRA activity (μmol g^{-1} FW h^{-1})
0.0
0.1
0.2
0.3
0.4
0.5
0.6
e
d
c
cd
b
a
Control
Severe
Extreme

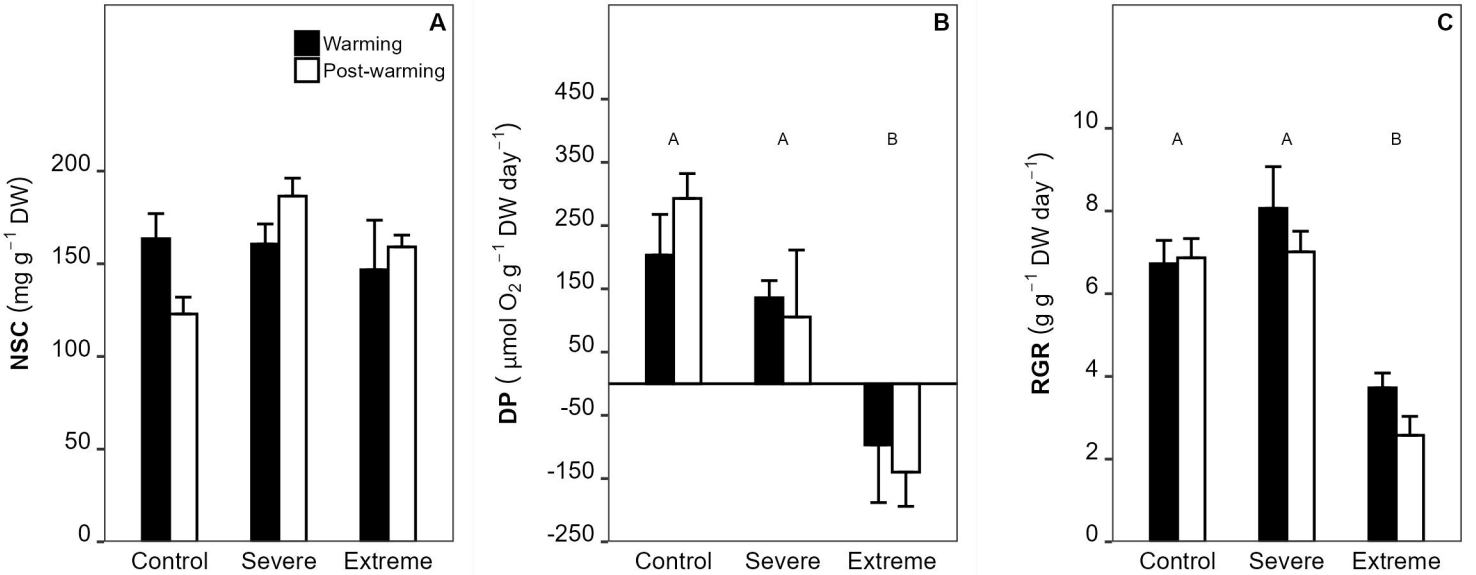
A
Warming
Post-warming
NSC (mg g^{-1} DW)
200
150
100
50
0
Control
Severe
Extreme
B
DP (µmol O_2 g^{-1} DW day^{-1})
450
350
250
150
50
-50
-150
-250
A
A
B
Control
Severe
Extreme
C
RGR (g g^{-1} DW day^{-1})
10
8
6
4
2
0
A
A
B
Control
Severe
Extreme

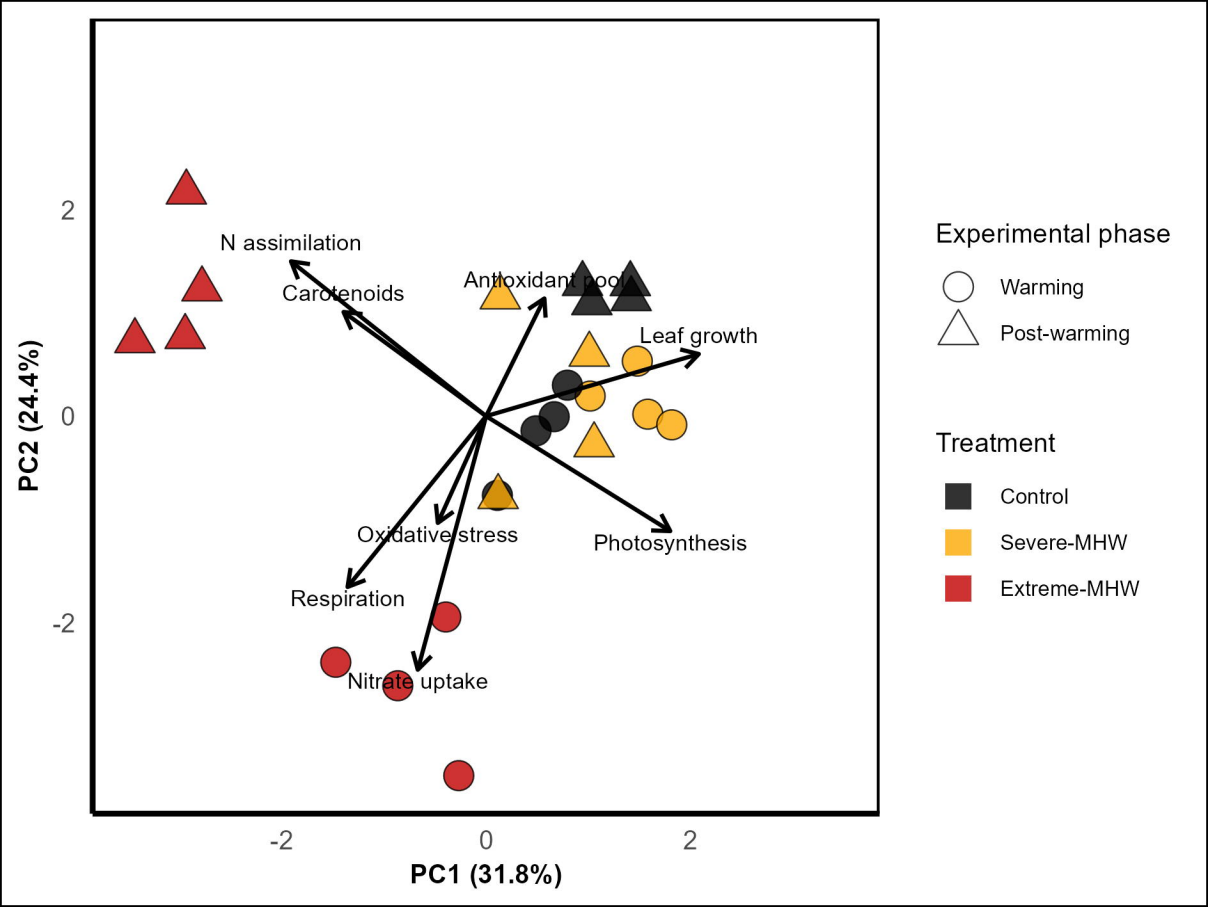
N assimilation
Carotenoids
Antioxidant pool
Leaf growth
Oxidative stress
Photosynthesis
Respiration
Nitrate uptake
PC1 (31.8%)
PC2 (24.4%)
2
0
-2
-2
0
2
Experimental phase
Warming
Post-warming
Treatment
Control
Severe-MHW
Extreme-MHW

Marine heatwaves exceed seagrass thermal limits

Vivanco-Bercovich et al., 2025

Seagrass meadow in Mexican Biosphere Reserve

Phyllospadix scouleri meadow, Isla Todos Santos, Baja California

From field to mesocosm

Experimental design

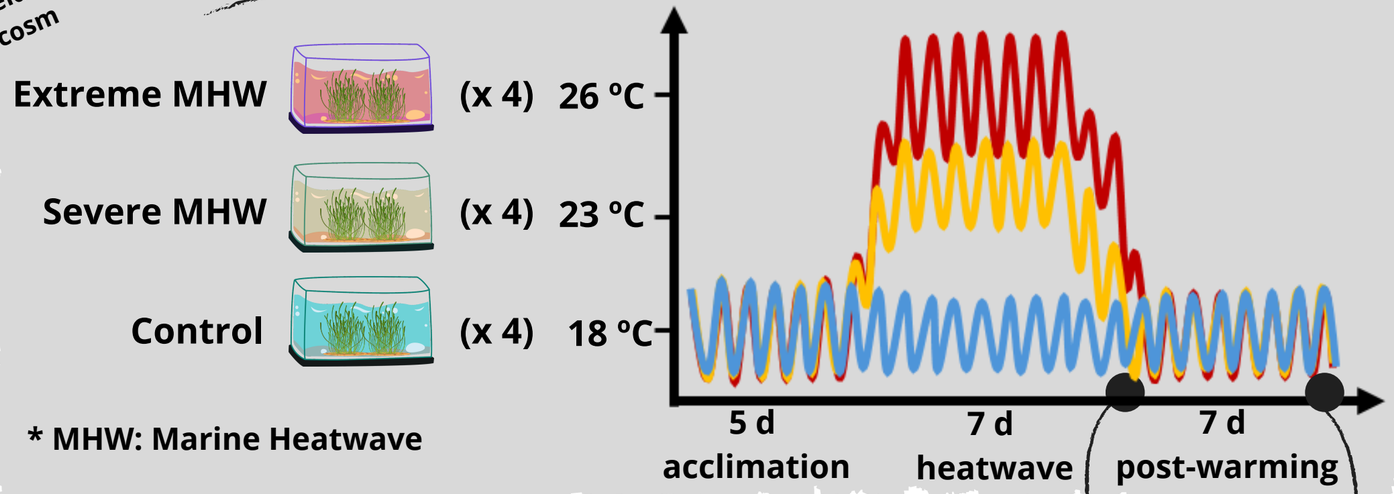

* MHW: Marine Heatwave

Samples from two time points

Physiological characterization

- Photosynthesis
- Respiration
- Pigments
- Oxidative stress
- N-assimilation
- C-balance
- Growth

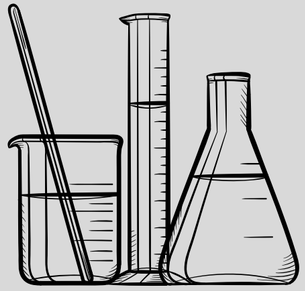

Conclusions

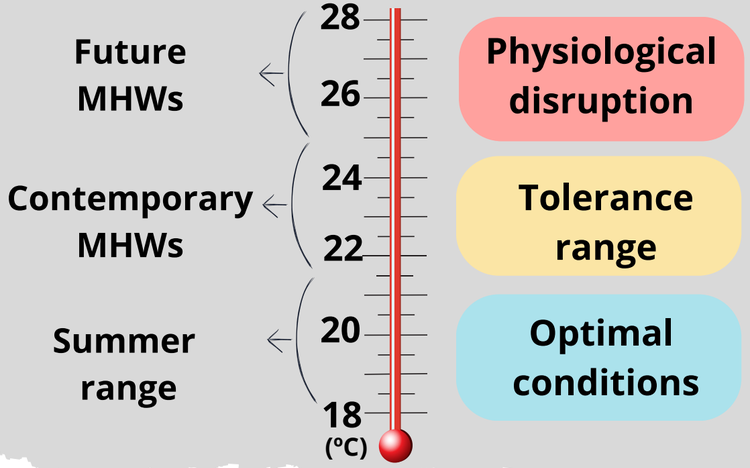

Key take-away

Extreme marine heatwaves (>26.5 °C) push *Phyllospadix scouleri* beyond its physiological limits, causing functional collapse and threatening its survival.